Published in final edited form as:
Genes Brain Behav. 2014 February ; 13(2): 179–194. doi:10.1111/gbb.12108.

Localization and Behaviors in Null Mice Suggest that ASIC1 and ASIC2 Modulate Responses to Aversive Stimuli

Margaret P. Price[1], **Huiyu Gong**[1], **Meredith G. Parsons**[1], **Jacob R. Kundert**[1], **Leah R. Reznikov**[1], **Luisa Bernardinelli**[2,3], **Kathryn Chaloner**[4], **Gordon F. Buchanan**[5,6], **John A. Wemmie**[7,8,13], **George B. Richerson**[9,10], **Martin D. Cassell**[11], and **Michael J. Welsh**[1,8,10,12]

[1]Department of Internal Medicine, Roy J. and Lucille A. Carver College of Medicine University of Iowa, Iowa City, Iowa 52242

[2]Department of Brain and Behavioral Sciences, University of Pavia Via Bassi 21, 27100 Pavia Italy

[3]Center of Biostatistics, Institute of Population Health, University of Manchester, Oxford Road, Manchester M13 9PL, United Kingdom

[4]Department of Biostatistics, College of Public Health University of Iowa, Iowa City, Iowa 52242

[5]Department of Neurology, Yale University School of Medicine New Haven, Connecticut, 06520

[6]Department of Neurology, Veteran's Affairs Medical Center West haven, Connecticut 06516

[7]Department of Psychiatry, Roy J. and Lucille A. Carver College of Medicine University of Iowa, Iowa City, Iowa 52242

[8]Department of Neurosurgery, Roy J. and Lucille A. Carver College of Medicine University of Iowa, Iowa City, Iowa 52242

[9]Department of Neurology, Roy J. and Lucille A. Carver College of Medicine University of Iowa, Iowa City, Iowa 52242

[10]Department of Molecular Physiology and Biophysics, Roy J. and Lucille A. Carver College of Medicine University of Iowa, Iowa City, Iowa 52242

[11]Department of Anatomy and Cell Biology, Roy J. and Lucille A. Carver College of Medicine University of Iowa, Iowa City, Iowa 52242

[12]the Howard Hughes Medical Institute Roy J. and Lucille A. Carver College of Medicine University of Iowa, Iowa City, Iowa 52242

[13]Department of Veterans Affairs Medical Center Iowa City, Iowa, 52242

Abstract

Acid sensing ion channels (ASICs) generate H^+-gated Na^+ currents that contribute to neuronal function and animal behavior. Like ASIC1, ASIC2 subunits are expressed in the brain and

Address correspondence to: Michael J Welsh Howard Hughes Medical Institute Carver College of Medicine, University of Iowa Department of Internal Medicine, 500 EMRB Iowa City, IA 52242 Phone 319-335-7619; FAX 319-335-7623 michael-welsh@uiowa.edu.

multimerize with ASIC1 to influence acid-evoked currents and facilitate ASIC1 localization to dendritic spines. To better understand how ASIC2 contributes to brain function, we localized the protein and tested the behavioral consequences of *ASIC2* gene disruption. For comparison, we also localized ASIC1 and studied *ASIC1*$^{-/-}$ mice. ASIC2 was prominently expressed in areas of high synaptic density, and with a few exceptions, ASIC1 and ASIC2 localization exhibited substantial overlap. Loss of ASIC1 or ASIC2 decreased freezing behavior in contextual and auditory cue fear conditioning assays, in response to predator odor, and in response to CO_2 inhalation. In addition, loss of ASIC1 or ASIC2 increased activity in a forced swim assay. These data suggest that ASIC2, like ASIC1, plays a key role in determining the defensive response to aversive stimuli. They also raise the question of whether gene variations in both *ASIC1* and *ASIC2* might affect fear and panic in humans.

Keywords

acid sensing ion channel; immunocytochemistry; ASIC1; ASIC2; brain; fear conditioning; carbon dioxide

INTRODUCTION

Acid sensing ion channels (ASICs) are non-voltage-gated Na^+ channels that open transiently when extracellular pH falls (Chu et al., 2011; Grunder and Chen, 2010; Sherwood et al., 2012). ASIC subunits form homo- and hetero-trimeric complexes (Jasti et al., 2007), and the combination of subunits determines pH-sensitivity, gating kinetics, and permeability (Benson et al., 2002; Hesselager et al., 2004). ASIC1a, ASIC2a, and ASIC2b are the main subunits expressed in murine brain neurons (Price et al., 1996; Waldmann et al., 1996). Electrophysiological studies indicate that H^+-gated currents in mouse central neurons are generated by a combination of ASIC1a homomultimers and ASIC1a/ASIC2a and ASIC1a/ASIC2b heteromultimers (Askwith et al., 2004; Chu et al., 2004; Gao et al., 2004; Jiang et al., 2009; Sherwood et al., 2011; Weng et al., 2010; Wu et al., 2004).

Most previous studies have focused on ASIC1 because it is required for acid-evoked ASIC currents at pH values >5 (Askwith et al., 2004; Wemmie et al., 2002). ASIC1 is located in dendrites and dendritic spines, as well as in cell bodies (Wemmie et al., 2002; Zha et al., 2009; Zha et al., 2006). ASIC1 is abundant in brain structures of the fear circuit (Coryell et al., 2007; Wemmie et al., 2003). Consistent with that localization, disrupting the *ASIC1* gene in mice causes deficits in acquired (context and cued fear conditioned assays) and innate (predator odor and CO_2 inhalation) fear-like behavior (Coryell et al., 2007; Wemmie et al., 2003; Ziemann et al., 2009). These abnormalities are manifested as reduced freezing behavior.

Much less is known about the localization and function of ASIC2 in the brain. Previous studies showed that ASIC2 can contribute to H^+-gated ASIC currents by multimerizing with ASIC1 (Askwith et al., 2004; Benson et al., 2002; Sherwood et al., 2011). In addition, we recently found that ASIC2 binds PSD95 and thereby facilitates localization of ASIC1/ASIC2 heteromultimeric channels to dendritic spines (Zha et al., 2009). Lack of either ASIC2 or ASIC1 reduced acid-evoked elevations of intracellular Ca^{2+} concentration,

$[Ca^{2+}]_i$, studied in dendritic spines of hippocampal neurons in brain slices. Recent genome-wide studies have associated SNPs near *ASIC2* with autism (Stone et al., 2007), panic disorder (Gregersen et al., 2012), response to lithium treatment in bipolar disorder (Squassina et al., 2011) and citalopram treatment in depressive disorder (Hunter et al., 2013), and have implicated a copy number variant of *ASIC2* with dyslexia (Veerappa et al., 2013). However, little is currently understood about whether ASIC2 is required for normal behavior.

The goals of this study were to better understand the role of ASIC2 in brain function. Thus our first aim was to localize ASIC2 subunits. Because ASIC2 subunits multimerize with ASIC1 subunits, we hypothesized that the distribution of the two subunits would show substantial overlap. In addition, given that ASIC channels in central neurons missing ASIC2 have altered trafficking and biophysical properties, we hypothesized that disrupting expression of ASIC2 would impact behavior. Therefore, we asked if mice missing ASIC2 would have altered behavioral phenotypes, and whether disrupting both *ASIC1* and *ASIC2* would have the same or greater behavioral effects than disrupting either gene alone. Because we found that ASIC2, like ASIC1, was highly expressed in brain regions that coordinate responses to threatening events, we focused on tests that evaluate defensive behaviors and reactions to stressful and aversive stimuli.

MATERIALS AND METHODS

Mice

We used $ASIC^{+/+}$, $ASIC1^{-/-}$, $ASIC2^{-/-}$, and $ASIC1/2^{-/-}$ mice on a congenic C57BL/6J background. The generation of *ASIC1* and *ASIC2 null* mice has been described (Price et al., 1996; Wemmie et al., 2002). Congenic $ASIC1^{-/-}$ and $ASIC2^{-/-}$ lines were crossed to one another to generate a congenic C57BL/6J line with the simultaneous disruption of *ASIC1* and *ASIC2* (*ASIC1/2 null* mice). $ASIC^{-/-}$ homozygous lines were refreshed every 5 generations by backcrossing to C57BL/6J $^{+/+}$ mice (Jackson Laboratory, Bar Harbor, Maine). $ASIC^{+/+}$ and $ASIC^{-/-}$ lines generated from these crosses were used in behavioral assays. Mice used in behavioral assays were group housed and matched for age (8 - 16 weeks). In some cases, the same set of mice was used in multiple behavioral assays. One set of mice was used in the fear conditioning assays (Fig. 8A, B, C, and E); one set of mice was used in the vigilance, arousal, and breathing assays (Fig. 9D, E, F, G, H, and I). Mice naive to testing were used for the remaining assays. We used both male and female mice; the number and gender used in behavioral assays are listed in the figure legends. All mouse behavioral assays were performed during the light cycle. All animal protocols were approved by the University of Iowa Institutional Animal Care and Use Committee.

Immunocytochemistry

A polyclonal anti-ASIC2 antibody (ISH-650) was generated in rabbits against a peptide containing the 21 carboxyl-terminal amino acids from mouse ASIC2, ISHTVNVPLQTALGTLEEIAC, coupled to keyhole limpet hemocyanin (AnaSpec, San Jose, CA). The IgG fraction was purified using immobilized Protein A (Thermo Fisher Scientific, Rockford, IL). This fraction was then passed over a column containing the

peptide immunogen covalently attached to Actigel ALD resin (Sterogene, Carlsbad, CA). After washing with phosphate-buffered saline (PBS), affinity-purified ASIC2-specific antibody was eluted with 100 mM glycine (pH 2.5) and neutralized with 1 M Tris base.

Brains were removed from young adult male animals euthanized by isoflurane inhalation, placed in molds containing optimal cutting temperature compound (Electron Microscopy Sciences, Hatfield, PA), and rapidly frozen by placing the molds in dry ice-chilled isopentane. Coronal (14 mm) or sagittal (12 mm) slices were cut and mounted on slides using a Microm Cryostat with a CryoJane tape-transfer system (Electron Microscopy Sciences, Hatfield, PA), postfixed in phosphate-buffered saline (PBS) containing 4% sucrose and 4% paraformaldehyde for 10 min at −20°C, and washed with PBS. Sections were then permeabilized with 0.25% triton X-100 in PBS for 5 min at 22°C, washed in PBS, and incubated in blocking buffer (Superblock) (Thermo Fisher Scientific) for 1 h at 22°C. For co-staining ASIC1 and −2, sections were incubated with goat anti-ASIC1 (1:300) (sc-13905 Santa Cruz Biotechnology, Santa Cruz, CA) and rabbit anti-ASIC2 ISH-650 (1:1000) primaries in blocking buffer overnight at 4°C. Following PBS wash, sections were placed in 5% normal donkey serum (Jackson ImmunoResearch, West Grove, PA) in PBS for 30 min at 22°C followed by incubation in either donkey anti-goat Alexa Fluor 488 (1:500) (A11055) or donkey anti-goat Alexa Fluor 568 (1:500) (A11057), and donkey anti-rabbit Alexa Fluor 488 (1:500) (A21206) or donkey anti-rabbit Alexa Fluor 568 (1:500) (A10042) (Alexa Fluor dyes - Life Technologies, Grand Island, NY) in 2% normal donkey serum (Jackson ImmunoResearch) in PBS for 45 min. Following wash in 0.1% triton X-100 in PBS and PBS rinse, the slides were mounted with VECTASHIELD HardSet Mounting Medium (Vector Laboratories, Burlingame, CA). For co-staining ASIC1 with glial fibrillary acidic protein (GFAP), sections were incubated with goat anti-ASIC1 (1:300) (Santa Cruz Biotechnology) and chicken anti-GFAP (1:500) (PA1-10004 Thermo Fisher Scientific). For co-staining ASIC2 with GFAP, sections were incubated with rabbit anti-ASIC2 ISH-650 (1:1000) and chicken anti-GFAP (1:500) (PA1-10004 Thermo Fisher Scientific).

A Zeiss LSM 710 confocal microscope (Carl Zeiss Microimaging, Inc., Thornwood, NY) was used to visualize the sections. Montage images of entire brain sections were acquired at 10X magnification using the Zeiss tile scanning function. NIH ImageJ software was used to produce final images.

Western Blot Analysis

Mouse brain sections from male mice were dissected and homogenized in RIPA (radioimmune precipitation assay) lysis buffer (Thermo Fisher Scientific) containing EDTA-free Halt Protease Inhibitor Cocktail (Thermo Fisher Scientific) using a glass/Teflon motor-driven homogenizer. Following ultracentrifugation (100,000 × *g* rpm) and analysis of protein concentration using the BCA assay kit (Thermo Fisher Scientific), 40 μg of protein were separated on 10% polyacrylamide-SDS gels (Criterion Tris-HCl precast gel) (Bio-Rad, Hercules, CA), and transferred to polyvinylidene fluoride (PVDF) Immobilon-FL membranes (Millipore, Billerica, MA). The membranes were blocked with casein blocking buffer (LI-COR Inc., Lincoln, NE), incubated for 2 h at room temperature in primary antibodies diluted in blocking buffer, washed 3 times with Tris-buffered saline containing

0.05% Tween (TTBS), and incubated for 40 min at room temperature in secondary antibodies diluted in blocking buffer plus 0.15% SDS followed by three washes in TTBS. The following primary antibodies were used: rabbit anti-ASIC2 ISH-650 (1:2000) described above; rabbit anti-ASIC1 MTY (1:3000) (Wemmie et al., 2003); goat anti-ASIC1 (1:200) (Santa Cruz Biotechnology); mouse anti-tubulin (1:15,000) (T5293 Sigma, St. Louis, MO)). The following secondary antibodies were used: donkey anti-rabbit IgG IRDye 800CW (1:10,000) (926-32213 LI-COR Inc.); donkey anti-mouse IgG IRDye 680 (1:10,000) (926-68022 LI-COR Inc.). Membranes were analyzed using an Odyssey infrared imaging system (LI-COR Inc.).

Context and cued fear conditioning

Experiments were performed as previously described (Sowers et al., 2013; Vralsted et al., 2011) utilizing a three day fear conditioning protocol (Anagnostaras et al., 2000; Israely et al., 2004) and computerized video fear conditioning system (Med Associates, St Albuns, VT). On Day1, mice were acclimated to the conditioning chamber for 3 min. Then, a 20 s tone (conditioned stimulus, 90 dB) was followed by a shock (0.75 mA, 1 s). The tone and shock were delivered 5 times with an 80 s interval. Freezing behavior was measured for 14 min. Freezing behavior was defined as the absence of movement other than respiration and was scored with VideoFreeze software (Med Associates). On Day 2, the contextual memory test was performed. Mice were placed in the training chamber, and freezing was assessed for 5 min. On Day 3, the cued (tone-dependent) memory test was performed in an environment with an altered appearance, floor texture, and odor. Three min after entering the chamber, there was a 3 min continuous tone (90 dB), followed by 4 min without tone. Freezing was assessed for each minute of the 10 min session.

Foot-shock sensitivity

Animals were exposed to 10 1-s foot-shocks delivered with an average intershock interval that varies randomly from a minimum of 10s to a maximum of 20 s apart at increasing intensities from 0.1 mA to 0.5 mA. Sensitivity to foot-shock was quantified by scoring the number of flinching responses (which include foot-lifting and head-twitching) out of ten presentations at each intensity.

Foot-shock response

The gross motor reactivity following foot-shock, referred to as the unconditioned activity burst, provides a measure of foot-shock or pain sensitivity (Anagnostaras et al., 1999). Using the Motion Index function (Video Freeze, Med Associates), the activity burst was quantified as the average activity during the first second following the initial foot-shock of the conditioning protocol during fear conditioning training. The activity burst is reported in arbitrary units. Previous studies have reported a linear relationship between the Motion Index measurement and the animal's mean velocity (cm/s) following foot-shock (Anagnostaras et al., 2000; Anagnostaras et al., 2010).

Predator odor-evoked behavior

Behaviors evoked by exposure to the fox feces odor, 2,5-dihydro-2,4,5-trimethylthiazoline (TMT) (300000368 Victoria, British Columbia, Canada) were quantified by placing mice in a Plexiglass assay chamber (19.7 cm deep × 16.5 cm tall × 19.7 cm wide) with a small beaker containing TMT (30 μL) or H_2O on a gauze pad. Freezing behavior was assessed during a 6 min period.

Olfactory Test

The ability to find buried food was assessed to test olfaction. Mice, fasted for 20 h, were allowed to explore a novel cage containing bedding material for 5 min. A food pellet approximately 2 cm long was buried under the bedding material. The mouse was allowed 15 min to find the hidden food pellet. The latency to find the food pellet was recorded.

CO_2-evoked behavior

Behaviors evoked by exposure to 10% CO_2 (flow-rate 5 L/min) (10% in 21% O2, balanced with N2) were quantified by placing mice in a Plexiglass chamber (19.1 cm deep × 14.6 cm tall × 18.4 cm wide). CO_2 was diffused into the chamber through small holes in the ceiling, while allowing CO_2 to diffuse out of the chamber through an outlet valve. Freezing behavior was assessed during a 10 min period.

EEG/EMG data acquisition and analysis

EEG/EMG headmounts (8201, Pinnacle Technology Inc., Lawrence, KS) and temperature/activity telemeters (G2 E-Mitter, Mini-Mitter, Inc., Bend, OR) were implanted under ketamine/xylazine anesthesia as previously described (Hodges et al., 2008). Animals were allowed to recover for at least 10 d before being studied. Animals were introduced to the recording chamber and allowed to acclimate as described below. Animals were fit with a small preamplifier (8202-SL Pinnacle Technology Inc., Lawrence, KS) attached directly to the implanted headmount. The preamplifier was connected to an amplifier (Model 440 Instrumentation Amplifier, Brownlee Precision Co.; San Jose, CA) by a tether and commutator (8204 Pinnacle Technology Inc.). Data were digitized with an analog-to-digital converter (PCI-6221 or USB-6008 National Instruments Corp., Austin, TX) and collected using software custom written in Matlab (Mathworks Co., Natick, MA). EEG signals were amplified by 50,000x and band-pass filtered from 0.3Hz to 200Hz. EMG signals were amplified by 50,000x and band-pass filtered from 10Hz to 10kHz. Data were manually scored in 10-sec epochs as waking (W), non-rapid eye movement sleep (NREM), or rapid eye movement sleep (REM) using software custom written in MatLab. Vigilance state was assigned using a standard approach (Buchanan and Richerson, 2010).

Twenty-four hour sleep recordings

Animals were acclimated to the recording setup and EEG tether for at least 18 h before starting the 24 h data collection period. Animals were kept in a modified home cage in a 12 h light:12 h dark lighting regimen for 24 h collections. Food and water was available *ad libitum*. The ambient temperature was maintained at 30 °C. EEG, EMG, and locomotor

activity were recorded and scored as above. All experiments were videotaped (AF20 Webcam, Logitech, Newark, CA) to aid in scoring of vigilance state.

Hypercapnic/Hypoxic challenges

Animals were placed into the 350 cm^3 Plexiglass recording chamber equipped with bedding, food, and water and allowed to acclimate for 2 h on 3 consecutive days prior to the actual experimental trial. The gas within the chamber at baseline was room air (RA; 21% O_2, 79% N_2), and was changed to hypercapnia (7% CO_2, 21% O_2, 72% N_2; 10 min) or hypoxia (5% O_2, 95% N_2; 2 min). After a baseline recording period in RA for at least 60 min, animals were exposed to either hypercapnia or hypoxia. Following exposure the gas within the chamber was changed back to RA for 20 min and then the animals were exposed to the other test gas mixture. Animals underwent 2 separate experimental trials spaced at least 4 d apart. Each test gas exposure was initiated after mice were noted to be asleep as determined by real-time observation of the streaming EEG/EMG traces, eye closure, and absence of motor activity. Flow rates were maintained at 710-760 ml/min with a flow meter (R-32004-10 or WU-32446-33 Cole-Parmer, Inc, Hoffman Estates, IL). All compressed gas containers were obtained from Airgas East (Cheshire, CT).

Elevated plus-maze

Animals were placed into the center of a cross-shaped maze elevated 91 cm from the floor with 2 open and 2 closed arms facing one of the open arms, and allowed to explore the maze freely for 5 min. The time that the animal spent in the open and closed arms and the number of entries into the closed arms were observed and quantified for a 5 min period.

Porsolt forced swim test

Animals, weighing between 20 and 25g, were placed in a 4 L plastic beaker containing water at 22°C. Animal behavior was observed for a 6 min period. The duration of immobility was scored. Movements necessary to keep the animal's head above water were not scored as mobility.

Open field test

The spontaneous activity of animals in an open space was assayed by tracking their movements in an open field apparatus (50.2 cm deep × 34.3 tall × 50.2 cm wide) (Viewpoint, Montreal, Canada) under bright illumination for 20 min. General motor ability (distance traveled) and anxiety-related behavior (time in center space, 21.0 cm × 18.4 cm area, 15.9 cm from outside edge of apparatus) were recorded using ViewPoint VideoTrack image software (ViewPoint Life Sciences, Montreal, Canada).

Barnes maze

A Barnes maze apparatus was used to assess the ability to learn the location of an escape box during 4 d of trials. The apparatus is a circular table with a diameter of 121.9 cm, 95.3 cm from the ground, where 44 −5.1 cm diameter holes are located equidistantly around the perimeter. Each hole is 54.6 cm from the center of the table. During the trial period, the escape box is placed under the escape hole (target hole). The escape hole is in a different

position for each mouse, but constant for each mouse over the 4 days of training. Each mouse was tested 4 times per day for 4 days, with a 15 min inter-trial interval separating each trial. Each trial began when the mouse was released from a position in the middle of the maze; each mouse was released facing the same direction. Each trial lasted up to 3 min or until the mouse entered the escape box. The mice who did not find the escape box within 3 min were guided to the correct hole. Once the mouse entered the box, it was allowed to remain in the box for 1 min. The latency to enter the target hole (acquisition) was automatically scored (ViewPoint Videotrack system and software). A probe trial was conducted on day 5 to determine if the animal could remember where the target hole was located by blocking the target hole and placing the animal on the maze. The length of time that the mouse spent in the quadrant containing the target hole (target quadrant) was compared to time spent in quadrants right, left, and opposite of the target quadrant.

Statistical analysis

Statistics were performed with R statistical software (R-Core-Team, 2013). Welch's two sample t-test was used to test for significant differences between two groups. One way analysis of variance (ANOVA) was used to assess differences in single factor experiments involving more than two groups and adjusted for sex. For ANOVA methods, Holm's method for multiple comparisons (Holm, 1979) was used to test relationships hypothesized between groups with a type I error rate for each assay set at 0.05. Linear mixed-effects models with a random effect for each mouse were used for the assays in Fig. 9 (G, H, I) to assess the effects of each of the 2-level factors. For the assay in Fig. 9D where there are three different responses constrained to a sum of 24 hours, generalized least squares was used to model two of the responses simultaneously, allowing for correlation. In Fig. 10G a mouse's latency response on each of 4 days was measured and generalized least squares again used, but allowing for a symmetric correlation structure between days for each mouse. For Fig. 8D, repeated measurements on the same mouse with a binomial response for the number of responses out of 10, the generalized estimating equation (GEE) method was used to estimate the effects in the logit scale of genotype and intensity. As the effect of intensity was not linear, and the interaction between genotype and intensity was highly significant, comparisons of $ASIC^{+/+}$ mice with other genotypes were made at each intensity, using the Bonferonni adjustment. The analyses of assays with more than one gender initially included both a sex effect and a sex by genotype interaction. In no assay was the sex by genotype interaction significant at level 0.05. In assays with no significant main effect of sex, sex was omitted as an explanatory variable. In the two assays where the main effect of sex was significant (Fig. 8A and Fig. 8C), the significant differences by genotype were adjusted for sex and the main effect of sex reported in Table S1. The results in figures are presented as means + SEM. A thorough description of statistical results can be found in Supplementary Table 1.

RESULTS

ASIC subunits are widely expressed in the brain

We immunolabeled ASIC subunits to better identify their expression patterns. As controls for specificity, we used mice with disrupted *ASIC1* and *ASIC2* genes ($ASIC1/2^{-/-}$). We

could not assess ASIC2 localization in the cerebellum because of nonspecific staining in *ASIC2*$^{-/-}$ mice. Figure 1A shows para-sagittal sections of wild-type and *ASIC1/2*$^{-/-}$ mouse brains costained for ASIC1 and ASIC2. As indicated by previous studies (Alvarez de la Rosa et al., 2003; Garcia-Anoveros et al., 1997; Lingueglia et al., 1997; Wemmie et al., 2003), both subunits were widely expressed. Enlarged images of specific regions are shown in Fig. 1B-1D as examples of the differential staining of ASIC1 and ASIC2 that occur throughout the brain. Here, we emphasize a few main points about the immunolocalization.

Immunostaining of ASIC1 and ASIC2 is most prominent in synaptically dense regions

Immunolabeling of both ASIC1 and ASIC2 was particularly prominent in the neuropil, areas comprised largely of dendrites and axons. For example, the main and accessory olfactory bulbs (MOB and AOB) are synaptically dense regions that process olfactory sensory signals into synaptic activity (Su et al., 2009). ASIC1 and ASIC2 showed intense immunostaining in the glomeruli (Fig. 2), which are spherical neuropil structures composed of axonal endings from olfactory receptor neurons and dendritic endings from mitral projection neurons and local interneurons. The glomeruli are among the nervous system structures with the highest density of synapses (Zou et al., 2009).

The neocortex is another synaptically dense region, and we found strong ASIC1 immunolabeling in cortical layers II/III (Fig. 3A, 3B). ASIC2 immunolabeling was prominent throughout most regions of the cortex. In addition, both ASIC1 and ASIC2 showed particularly intense staining in the retrosplenial area of the cingulate cortex (RSCx) (Fig. 3C).

Areas of the brainstem that have integrative functions also showed strong ASIC1 and ASIC2 immunostaining (Fig. 3D, 3E, 3F). These include areas that produce serotonin (dorsal and medial raphe, DR and MNR), acetylcholine (lateral dorsal tegmental nucleus, LDTg), and norepinephrine (locus cerulius, LC). ASIC1 and ASIC2 also showed pronounced staining in additional brainstem structures that function in the coordinated control of autonomic function (nucleus of the solitary tract, NTS) and motor behavior (inferior olive, IO).

A recent study suggested that ASICs might be expressed in astrocytes as well as in neurons (Huang et al., 2010). To test this possibility, we co-localized ASIC1 and ASIC2 with glial fibrillary acidic protein (GFAP), a marker for astrocytes, in brain regions where ASIC1 and ASIC2 are highly expressed (Fig. 4). However, we did not see significant co-localization.

ASIC1 and ASIC2 show differential localization in some regions

Although ASIC1 and ASIC2 largely co-localized, there were areas where one or the other labeled much more prominently. The schematics in Fig. 5 show the relative immunostaining of ASIC1 and ASIC2 in various brain regions. Because this model is based on immunostaining data, we cannot make conclusions about the absolute abundance of the subunits or about the amount of one subunit *vs*. the other. However, the data do suggest relative differences in ASIC1 and ASIC2 protein in various brain regions.

An example is in the olfactory bulb; immunolabeling in the external plexiform layer of the main olfactory bulb appeared to be almost exclusively ASIC2 (Fig. 1B, 2). The external

plexiform layer (EPl) is nearly all neuropil consisting of dendrites from the mitral, tufted, and granule cells from deeper layers. Other areas where ASIC2 staining predominated included the median preoptic nucleus (MnPO) (Fig. 3A), the reticular thalamic nucleus (RT) (Fig. 3B), the lacunosum moleculare and oriens layers of the dorsal (Fig. 3B) and ventral hippocampus (Hi) (Fig. 3C), the anterior-medial portion of the bed nucleus of the stria terminalis (BST) (Fig. 6), the interpeduncular nucleus (IP) (Fig. 1A, 1D, 3C), the parasubiculum (PaS) (Fig. 3D), the rhabdoid nucleus (Rbd) (Fig. 3D), and the dorsal raphe nuclei (DR) (Fig. 3D).

There were also areas where ASIC1 immunostaining predominated with little if any ASIC2 staining. These included the lateral habenula (LHb) (Fig. 3B), the caudate and putamen (CPu) (Fig. 3A), the median raphe nuclei (MnR) (Fig. 3D), and the hypoglossal nucleus (12N) (Fig. 3F).

The immunolocalization pattern of ASIC1 and ASIC2 throughout the brain generally agrees with western blot analysis of the relative abundance of the two proteins in various brain regions (Fig. 7A, 7B). ASIC1 levels appeared to be highest in the amygdala and frontal cortex, and ASIC2 levels appeared to be highest in the frontal cortex and olfactory bulb. ASIC2 was barely detectable in the cerebellum. Western blot analysis of whole brain lysate from *ASIC*$^{+/+}$, *ASIC1*$^{-/-}$, and *ASIC2*$^{-/-}$ mice with anti-ASIC1 and anti-ASIC2 antibodies (Fig. 7C) showed that the major bands recognized by ASIC1 and ASIC2 antibodies corresponded to the expected protein sizes; the minor bands may represent forms of the proteins that differ in extent of phosphorylation or glycosylation or are degradation products.

The habenula/interpeduncular pathway has the most intense ASIC staining

ASIC immunolabeling was greatest in the habenular-interpeduncular pathway. Both subunits showed intense staining in the medial habenula (Fig. 3B). The most pronounced ASIC2 staining was in the interpeduncular nucleus (IP) (Fig. 1A, 1D, 3C). The medial habenula receives input from limbic brain structures, and sends outputs to the interpeduncular nucleus (IP); these projections represent a major cholinergic pathway. The IP in turn regulates activity of serotonergic neurons through projections to the raphe nuclei (Lecourtier and Kelly, 2007). The lateral habenula showed prominent ASIC1 immunolabeling, whereas ASIC2 was not detected there (Fig. 3B). The lateral habenula receives inputs from the basal ganglia and limbic structures and sends outputs through the rostromedial tegmental nucleus (RMTg) to dopaminergic, serotonergic, and noradrenergic neurons to regulate their firing following aversive and stressful events and reward omission (Lavezzi and Zahm, 2011). Expression of ASIC1 and ASIC2 in the habenular-interpeduncular circuit suggests that both subunits may contribute to neural systems that regulate monoamine levels in the brain.

ASIC1 and ASIC2 are localized in structures associated with fear-like responses

Our previous work identified ASIC1 expression in structures associated with fear, and behavioral studies implicated ASIC1 in the expression of conditioned and unconditioned fear-like behaviors (Coryell et al., 2007; Wemmie et al., 2003). Like ASIC1, we found prominent ASIC2 immunostaining in the basolateral nucleus (BLA) and the two main

components of the central extended amygdala, the central nucleus (CeA) (Fig. 3B) and the bed nucleus of the stria terminalis (BST) (Fig. 3A), with particularly intense ASIC2 immunostaining in the anterior-medial portion of the BST (BSTam) (Fig. 6). This region innervates neurosecretory neurons that synthesize corticotropin releasing hormone in the paraventricular nucleus of the hypothalamus (PVN) (Dong and Swanson, 2006). ASIC2 staining was also pronounced in the CA2 area of the hippocampus (Fig. 3B). CA2 has connections to the PVN and hypothalamic supramammilary nucleus, areas activated in response to threatening stimuli and important in modulating stress-related alterations in learning and memory (Choi et al., 2012; Cui et al., 2013). We further detected ASIC1 and ASIC2 in all regions of the periaqueductal gray (PAG) (Fig. 3D), where ASIC1 may contribute to innate fear-like behaviors (Coryell et al., 2007). Stimulation of the dorsolateral PAG evokes arousal, tachycardia, increased blood pressure and respiration, analgesia, and increased motor activity as in a fight or flight response. In contrast, stimulation of neurons in the ventrolateral PAG causes an immobility as in freezing evoked by aversive stimuli (Johnson et al., 2004).

ASIC1$^{-/-}$ and ASIC2$^{-/-}$ mice have reduced freezing in conditioned and innate fear assays

Prominent ASIC subunit expression in the amygdala, BST, and PAG suggested that ASICs could play prominent roles in the response to aversive stimuli and its associated motor activity. Our previous work showed that ASIC1 is required for normal learned freezing in response to the fox feces predator odor, 2,5-dihydro-2,4,5-trimethylthiazoline (TMT) (Coryell et al., 2007; Wemmie et al., 2003). Therefore, we studied *ASIC1*$^{-/-}$, *ASIC2*$^{-/-}$, and *ASIC1/2*$^{-/-}$ mice in a series of tests that assess fear-like behavior.

In the fear conditioning assay, mice were trained to associate an auditory cue and a novel environment (context) with a foot-shock, and we measured freezing behavior. During the training period, *ASIC1*$^{-/-}$, *ASIC2*$^{-/-}$ and *ASIC1/2*$^{-/-}$ mice had reduced freezing responses ($F_{3,84} = 16.22$, $P = 2.11 \times 10^{-8}$) (Fig. 8Aa). There was no statistically significant sex by genotype interaction, however a significant effect of sex was detected ($F_{1,84} = 4.86$, $P = 0.03$) (Fig. 8Ab; females froze for 37 s longer than males (Table S1). Compared to wild-type controls, all three *ASIC null* genotypes showed reduced freezing in response to context ($F_{3,71} = 14.36$, $P = 2.08 \times 10^{-7}$) (Fig. 8B). Compared to wild-type controls, all three *ASIC null* genotypes also showed reduced freezing in response to cue ($F_{3,84} = 28.89$, $P = 6.25 \times 10^{-13}$) (Fig. 8Ca); *ASIC2*$^{-/-}$ mice showed a significantly smaller deficit than *ASIC1*$^{-/-}$ or *ASIC1/2*$^{-/-}$ animals. There was no statistically significant sex by genotype interaction, however a significant effect of sex was detected ($F_{1,84} = 3.98$, $P = 0.049$) (Fig. 8Cb); females froze for 20 s longer than males (Table S1). The deficits in freezing were not due to an inability to detect a foot-shock because all genotypes had similar flinching behavior with increasing intensities of foot-shock except at 0.20 mA and 0.25 mA where *ASIC1/2*$^{-/-}$ mice showed a slightly greater response than *ASIC*$^{+/+}$ (GEE, $\chi^2_{24} = 436$, $P = 0.00026$ for genotype by intensity interaction) (Fig. 8D). In fact, *ASIC1*$^{-/-}$ and *ASIC1/2*$^{-/-}$ animals showed an enhanced activity burst following the initial foot-shock of the training protocol ($F_{3,84} = 4.89$, $P = 0.0035$) (Fig. 8E). Previous studies have also shown that *ASIC2*$^{-/-}$ mice have normal hearing and vision (Ettaiche et al., 2004; Peng et al., 2004; Roza et al., 2004).

The enhanced activity burst of *ASIC1*$^{-/-}$ and *ASIC1/2*$^{-/-}$ mice following foot-shock was unexpected, particularly since targeting ASIC1a in wild-type animals with intrathecal delivery of antisense oligonucleotides or peptide venoms produced analgesic effects (Deval et al., 2010; Diochot et al., 2012; Mazzuca et al., 2007). However, ASIC1a does not influence all pain behaviors (Page et al., 2004; Walder et al., 2010). Moreover, deficits in foot-shock sensitivity in *ASIC1*$^{-/-}$ or *ASIC2*$^{-/-}$ animals have not previously been reported. Our immunostaining studies showed ASIC1 expression in PAG and hypothalamic nuclei, areas that elicit appropriate freezing and/or escape behaviors in response to unconditioned nociceptive stimuli such as foot-shock (Sewards and Sewards, 2002). The enhanced reactivity to foot-shock in global *ASIC1*$^{-/-}$ and *ASIC1/2*$^{-/-}$ animals may thus reflect ASIC1 function in specific brain areas that modulate defensive responses to painful stimuli.

As a test of innate fear-like behavior, we measured the response to TMT (Takahashi et al., 2005). *ASIC1*$^{-/-}$, *ASIC2*$^{-/-}$ and *ASIC1/2*$^{-/-}$ mice exhibited reduced freezing compared to wild-type controls ($F_{3,27} = 7.44$, $P = 0.00089$) (Fig. 9A). In contrast, mice of all genotypes found a buried food pellet with similar latency ($F_{3,32} = 0.43$, $P = 0.74$) (Fig 9B), suggesting that there was not a general deficit in olfaction.

Inhaling CO_2 reduces brain pH, induces fear-like behavior in rodents (Mongeluzi et al., 2003; Ziemann et al., 2009), and can induce panic in humans (Feinstein et al., 2013; Gorman et al., 1994). Compared to wild-type mice, *ASIC1*$^{-/-}$, *ASIC2*$^{-/-}$, and *ASIC1/2*$^{-/-}$ animals showed less freezing in 10% CO_2 ($F_{3,52} = 17.67$, $P = 4.9 \times 10^{-8}$) (Fig. 9C). Mice did not freeze when placed in the testing box in the absence of CO_2 (data not shown).

The altered CO_2-induced freezing raised questions about other CO_2-dependent responses, such as CO_2-induced arousal from sleep and the hypercapnic ventilatory response. Wild-type and *ASIC1/2*$^{-/-}$ mice spent similar amounts of time awake and sleeping as assessed by video EEG and EMG during a 12 hr/12 hr light/dark cycle (generalized least squares, $F_{1,29} = 3.08$, $P = 0.09$) (Fig. 9D). The latency to arousal when sleeping mice were exposed to 7% CO_2 or 5% O_2 revealed no statistically significant genotype-dependent difference ($t_{13.91} = -0.94$, $P = 0.36$) (Fig. 9E), ($t_{9.50} = -1.43$, $P = 0.19$) (Fig. 9F). Arousal latencies were similar to those reported for wild-type mice (Buchanan and Richerson, 2010). In addition, there was no significant difference between *ASIC*$^{+/+}$ and *ASIC1/2*$^{-/-}$ mice in breathing frequency, tidal volume, or minute ventilation, or in changes in these parameters induced by CO_2 (linear mixed model with a random effect for mouse, ($F_{1,13} = 0.11$, $P = 0.75$) (Fig. 9G), ($F_{1,13} = 3.09$, $P = 0.1$) (Fig. 9H), ($F_{1,13} = 1.89$, $P = 0.19$) (Fig. 9I). Because we did not see differences between *ASIC*$^{+/+}$ and *ASIC1/2*$^{-/-}$ mice, we did not further analyze ASIC single knockout animals in these assays.

ASIC1$^{-/-}$ and *ASIC2*$^{-/-}$ mice show increased mobility in the forced swim assay

In the Porsolt forced swim test (Porsolt et al., 1977), we placed mice in a beaker of water. In this assay, mice try to escape the aversive stimulus by swimming, and they then begin to float. Increased floating has been attributed to a depression-like phenotype (Crawley, 1999). Compared to wild-type mice, *ASIC1*$^{-/-}$, *ASIC2*$^{-/-}$, and *ASIC1/2*$^{-/-}$ mice exhibited prolonged activity, and thus the time spent immobile decreased ($F_{3,99} = 14.02$, $P = 1.1 \times 10^{-7}$) (Fig. 10A). *ASIC1/2*$^{-/-}$ mice displayed a small statistically significant difference in

mobility from the *ASIC1*$^{-/-}$, but the biological significance of this is unclear. The increased time that *ASIC*$^{-/-}$ mice spent swimming is consistent with enhanced active behavior when challenged (Warden et al. 2012).

ASIC1$^{-/-}$ and *ASIC2*$^{-/-}$ mice show normal responses in some behavioral tests

Finding that *ASIC null* mice had less freezing in acquired and innate fear assays, increased reactivity to foot-shock, and enhanced mobility to swim stress led us to additional tests of behavior that might provide a less intense aversive stimulus.

Open field and elevated plus maze assays provide tests for anxiety-like behavior. In an open field assay, time spent exploring the open center area is interpreted as a measure of reduced anxiety-like behavior. *ASIC1*$^{-/-}$, *ASIC2*$^{-/-}$, and *ASIC1/2*$^{-/-}$ animals did not differ significantly from *ASIC*$^{+/+}$ in the time spent in the center ($F_{3,91} = 4.28$, $P = 0.0071$) (Fig. 10B). However, the *ASIC1*$^{-/-}$ animals showed a trend toward spending more time in the center of the open field than did *ASIC*$^{+/+}$ mice, and they differed significantly from *ASIC2*$^{-/-}$ animals. The total distance travelled did not differ between genotypes ($F_{3,91} = 1.11$, $P = 0.35$) (Fig. 10C). In an elevated plus maze, mice choose between exploring the open arms of a maze with no walls or closed arms with walls. The percentage of time spent in open and closed arms and the number of entries into closed arms did not differ by genotype ($F_{3,35} = 0.09$, $P = 0.97$) (Fig. 10D), ($F_{3,35} = 2.48$, $P = 0.078$) (Fig. 10E), ($F_{3,35} = 1.009$, $P = 0.4$) (Fig. 10F). Both the open field and elevated plus maze assays test the animal's innate avoidance of bright, open environments. The lack of a strong difference between ASIC$^{-/-}$ and ASIC$^{+/+}$ animals in time spent in the center of the open field and no difference in time spent in the open arm of the elevated plus maze suggest that ASICs do not play a large role in influencing fear of open and elevated spaces.

As a test of hippocampus-dependent learning, we used the circular Barnes maze task, which requires spatial memory to find an escape hole located among 43 other holes around the circumference of a circular table. Wild-type, *ASIC1*$^{-/-}$, *ASIC2*$^{-/-}$, and *ASIC1/2*$^{-/-}$ mice all showed similar acquisition of memory for the position of the escape hole during the 4 day training period (generalized least squares, $F_{3,173} = 0.69$, $P = 0.56$) (Fig. 10G). During the probe test on day 5, there were no statistically significant differences between genotypes in time spent in any of the quadrants either containing the escape hole ($F_{3,37} = 1.19$, $P = 0.33$), left of the escape hole ($F_{3,37} = 0.09$, $P = 0.97$), opposite the escape hole ($F_{3,37} = 0.62$, $P = 0.60$), or to the right of the escape hole ($F_{3,37} = 1.3$, $P = 0..30$) (Fig. 10H).

DISCUSSION

ASIC1 and ASIC2 show both overlapping and distinct localizations

In many brain regions, ASIC1 and ASIC2 co-localized, and in a few areas ASIC1 stained more intensely than ASIC2. These data are consistent with electrophysiological studies of cultured brain neurons that have revealed H^+-gated currents with biophysical properties of ASIC1/ASIC2 heteromultimers and ASIC1 homomultimers (Askwith et al., 2004; Chu et al., 2004; Gao et al., 2004; Jiang et al., 2009; Sherwood et al., 2011; Weng et al., 2010; Wu et al., 2004). However, we also observed some areas with pronounced ASIC2 staining with

little detectable ASIC1 staining. This result seemed surprising; whereas ASIC1 homomultimers and ASIC1/ASIC2 heteromultimers respond to H^+ in the physiological range, ASIC2 homomultimeric channels require pH less than 5 to open (Babinski et al., 2000; Benson et al., 2002; Lingueglia et al., 1997). In addition, currents consistent with ASIC2 homomultimers have not yet been identified in central neurons (Askwith et al., 2004; Sherwood et al., 2011; Weng et al., 2010). These observations raise the question of whether ASIC2 might be regulated by as yet undiscovered ligands; the recent finding that ASIC2 channels are markedly potentiated by a coral snake toxin hints that this might be the case (Bohlen et al., 2011).

Many of the areas that show robust ASIC1 and ASIC2 immunostaining were associated with cholinergic systems. For example, both subunits were abundantly expressed in the medial habenula, medial septum, and olfactory glomeruli - areas that contain a high number of nicotinic cholinergic receptors. In addition, the subunits show some separation in regions rich in nicotinic vs. muscarinic cholinergic receptors. Areas displaying dominant ASIC2 staining - the reticular thalamic nucleus, IPN, parasubiculum - show close correlation with nicotinic receptors, whereas areas with dominant ASIC1 staining - the lateral habenula, caudate and putamen, hypoglossal nucleus - show better correlation with muscarinic receptors. The association of ASIC1 and ASIC2 with these systems suggests that ASICs may influence neurotransmission in cholinergic pathways.

Lack of ASIC1 and/or ASIC2 reduces freezing and immobility in some assays and enhances activity in others

Disrupting either the *ASIC1* or *ASIC2* gene reduced the freezing response in tests of acquired (cued and context fear conditioning) and innate (TMT and CO_2) fear-like behavior. Moreover, the response in *ASIC1/2*$^{-/-}$ mice was generally not greater than with the disruption of *ASIC1* or *ASIC2* alone. These phenotypic similarities may be explained by the overlapping localization of ASIC1 and ASIC2 in the amygdala, BST, and PAG and the finding that ASIC2 binding to PSD95 facilitates ASIC1 movement to dendritic spines (Zha et al., 2009). However in cued fear conditioning, *ASIC2*$^{-/-}$ mice showed a smaller deficit to an auditory cue than *ASIC1*$^{-/-}$ or *ASIC1/2*$^{-/-}$ animals. Possible explanations are that the H^+ sensitivity or kinetics of ASIC1 channels might be key for this response or that ASIC1 homomeric channels might make a more substantial contribution to cued fear conditioning than ASIC1/ASIC2 heteromeric channels.

ASIC channels influence behavior in response to intense, aversive stimuli

When *ASIC* genes were disrupted, behavioral tests that involved substantial aversive stimuli became abnormal; examples include foot-shock in fear conditioning assays, forced swim in a beaker of water, exposure to a predator odor, and inhalation of a high CO_2 concentration. In contrast, behavior of *ASIC null* and wild-type mice did not differ significantly in tests that involved a stimulus that may be less stressful; examples include exposure to an open field, placement on the arms of an elevated plus maze, and testing arousal from sleep with exposure to gas containing increased CO_2 or reduced O_2. These results suggest that *ASIC1*$^{-/-}$, *ASIC2*$^{-/-}$, and *ASIC1/2*$^{-/-}$ mice manifest behavioral defects primarily when the

aversive or stressful stimulus is very intense. The patterns of ASIC subunit localization together with earlier studies suggest an explanation for these findings.

First, the most prominent ASIC1 and ASIC2 immunostaining occurred in areas of high synaptic density, which suggests that these subunits play a role in synaptic transmission. That conclusion is consistent with previous studies in brain slices and cultured neurons that localized ASIC1 and ASIC2 at dendritic spines (Wemmie et al., 2006; Zha et al., 2009; Zha et al., 2006). In addition, ASIC1 and ASIC2 were enriched in synaptosomal membrane preparations (Wemmie et al., 2002; Wemmie et al., 2004; Zha et al., 2009) and associated with postsynaptic scaffolding proteins (Duggan et al., 2002; Hruska-Hageman et al., 2002; Xu and Xiong, 2007; Zha et al., 2009). Thus, the data suggest that ASIC1 and ASIC2 sit in the postsynaptic membrane.

Second, neither ASIC1 nor ASIC2 are required for synaptic transmission under basal conditions. For example, we previously showed that hippocampal excitatory postsynaptic potentials did not differ between *ASIC1*$^{-/-}$ and wild-type mice under basal conditions (Wemmie et al., 2002). Moreover, *ASIC1*$^{-/-}$, *ASIC2*$^{-/-}$, and *ASIC1/2*$^{-/-}$ mice have many normal behaviors even though ASIC subunits are present in brain structures that influence the behaviors.

Third, pH can fall with synaptic activity and ASIC channels are activated when pH falls. Previous work in hippocampal slices showed that synaptic transmission can induce a rapid extracellular acidification and sequential stimuli enhanced the reduction in pH (Krishtal et al., 1987). Synaptic transmission at ribbon synapses in mammalian cone photoreceptors also reduced extracellular pH (DeVries, 2001). Moreover, a recent magnetic resonance imaging study showed that pH fell in the visual cortex of people viewing a bright flashing checkerboard (Magnotta et al., 2012). Numerous studies have shown that protons activate both recombinant and endogenous ASIC1 homomultimers and ASIC1/ASIC2 heteromultimers (Askwith et al., 2004; Sherwood et al., 2011; Weng et al., 2010). In earlier work, we also showed that reducing the pH of a hippocampal brain slice increased $[Ca^{2+}]_i$ in dendritic spines, and the response depended on ASIC1 and ASIC2 (Zha et al., 2009; Zha et al., 2006).

These results suggest that ASIC channels can influence synaptic transmission. We speculate that pH falls to the greatest extent with intense synaptic activity; the mechanism might involve release of the acidic contents of synaptic vesicles, transport of HCO_3^- or H^+ across neuronal or glial cell membranes, and/or metabolism. The reduced pH could activate ASIC channels leading to an increased $[Ca^{2+}]_i$ (Xiong et al., 2004; Yermolaieva et al., 2004; Zha et al., 2006). In this scenario, the main function of ASIC channels would be to enhance synaptic transmission in response to intense activity. This would explain the pattern of abnormal behavior in *ASIC null* mice when the stimulus is very aversive.

Supplementary Material

Refer to Web version on PubMed Central for supplementary material.

Acknowledgments

This work was supported in part by Fondazione Cariplo grant 2009-2528, and by FISM -Fondazione Italiana Sclerosi Multipla grant 2009/R/ 2. LRR is supported by the Iowa Cardiovascular Interdisciplinary Research Fellowship (HL07121). JAW is supported by the Department of Veterans Affairs (Merit Award) and the National Institutes of Mental Health (1R01MH085724-01), National Institutes of Mental Health (1R01MH085724-01), National Institute of Heart Lung and Blood (5 R01 HL113863-01), and a McKnight Neuroscience of Brain Disorders Award. MT is supported by the National Institutes of Health (NIH) Clinical and Translational Science Award (CTSA) program, grant 2 UL1 TR000442-06. MJW is a Howard Hughes Medical Institute Investigator. We thank Thomas Moninger, Monelle Tamegnon, Erin Bagnall, Kyle Heffernan, Mackenzie Treolar, Mara Zuckerman, and Luisa Foco for excellent assistance. We thank the University of Iowa Office of Animal Resources and the Central Microscopy Research Facility.

REFERENCES

Alvarez de la Rosa D, Krueger SR, Kolar A, Shao D, Fitzsimonds RM, Canessa CM. Distribution, subcellular localization and ontogeny of ASIC1 in the mammalian central nervous system. J Physiol. 2003; 546:77–87. [PubMed: 12509480]

Anagnostaras SG, Josselyn SA, Frankland PW, Silva AJ. Computer-assisted behavioral assessment of Pavlovian fear conditioning in mice. Learn Mem. 2000; 7:58–72. [PubMed: 10706603]

Anagnostaras SG, Maren S, Sage JR, Goodrich S, Fanselow MS. Scopolamine and Pavlovian fear conditioning in rats: dose-effect analysis. Neuropsychopharmacology. 1999; 21:731–744. [PubMed: 10633479]

Anagnostaras SG, Wood SC, Shuman T, Cai DJ, Leduc AD, Zurn KR, Zurn JB, Sage JR, Herrera GM. Automated assessment of pavlovian conditioned freezing and shock reactivity in mice using the video freeze system. Front Behav Neurosci. 2010; 4

Askwith CC, Wemmie JA, Price MP, Rokhlina T, Welsh MJ. Acid-sensing ion channel 2 (ASIC2) modulates ASIC1 H+-activated currents in hippocampal neurons. J Biol Chem. 2004; 279:18296–18305. [PubMed: 14960591]

Babinski K, Catarsi S, Biagini G, Seguela P. Mammalian ASIC2a and ASIC3 subunits co-assemble into heteromeric proton-gated channels sensitive to Gd3+. J Biol Chem. 2000; 275:28519–28525. [PubMed: 10842183]

Benson CJ, Xie J, Wemmie JA, Price MP, Henss JM, Welsh MJ, Snyder PM. Heteromultimers of DEG/ENaC subunits form H+-gated channels in mouse sensory neurons. Proc Natl Acad Sci U S A. 2002; 99:2338–2343. [PubMed: 11854527]

Bohlen CJ, Chesler AT, Sharif-Naeini R, Medzihradszky KF, Zhou S, King D, Sanchez EE, Burlingame AL, Basbaum AI, Julius D. A heteromeric Texas coral snake toxin targets acid-sensing ion channels to produce pain. Nature. 2011; 479:410–414. [PubMed: 22094702]

Buchanan GF, Richerson GB. Central serotonin neurons are required for arousal to CO2. Proc Natl Acad Sci U S A. 2010; 107:16354–16359. [PubMed: 20805497]

Choi WK, Wirtshafter D, Park HJ, Lee MS, Her S, Shim I. The characteristics of supramammillary cells projecting to the hippocampus in stress response in the rat. Korean J Physiol Pharmacol. 2012; 16:17–24. [PubMed: 22416215]

Chu XP, Papasian CJ, Wang JQ, Xiong ZG. Modulation of acid-sensing ion channels: molecular mechanisms and therapeutic potential. Int J Physiol Pathophysiol Pharmacol. 2011; 3:288–309. [PubMed: 22162785]

Chu XP, Wemmie JA, Wang WZ, Zhu XM, Saugstad JA, Price MP, Simon RP, Xiong ZG. Subunit-dependent high-affinity zinc inhibition of acid-sensing ion channels. J Neurosci. 2004; 24:8678–8689. [PubMed: 15470133]

Coryell MW, Ziemann AE, Westmoreland PJ, Haenfler JM, Kurjakovic Z, Zha XM, Price M, Schnizler MK, Wemmie JA. Targeting ASIC1a reduces innate fear and alters neuronal activity in the fear circuit. Biol Psychiatry. 2007; 62:1140–1148. [PubMed: 17662962]

Crawley JN. Behavioral phenotyping of transgenic and knockout mice: experimental design and evaluation of general health, sensory functions, motor abilities, and specific behavioral tests. Brain Res. 1999; 835:18–26. [PubMed: 10448192]

Cui Z, Gerfen CR, Young WS 3rd. Hypothalamic and other connections with dorsal CA2 area of the mouse hippocampus. J Comp Neurol. 2013; 521:1844–1866. [PubMed: 23172108]

Deval E, Gasull X, Noel J, Salinas M, Baron A, Diochot S, Lingueglia E. Acid-sensing ion channels (ASICs): pharmacology and implication in pain. Pharmacol Ther. 2010; 128:549–558. [PubMed: 20807551]

DeVries SH. Exocytosed protons feedback to suppress the Ca2+ current in mammalian cone photoreceptors. Neuron. 2001; 32:1107–1117. [PubMed: 11754841]

Diochot S, Baron A, Salinas M, Douguet D, Scarzello S, Dabert-Gay AS, Debayle D, Friend V, Alloui A, Lazdunski M, et al. Black mamba venom peptides target acid-sensing ion channels to abolish pain. Nature. 2012; 490:552–555. [PubMed: 23034652]

Dong HW, Swanson LW. Projections from bed nuclei of the stria terminalis, anteromedial area: cerebral hemisphere integration of neuroendocrine, autonomic, and behavioral aspects of energy balance. J Comp Neurol. 2006; 494:142–178. [PubMed: 16304685]

Duggan A, Garcia-Anoveros J, Corey DP. The PDZ domain protein PICK1 and the sodium channel BNaC1 interact and localize at mechanosensory terminals of dorsal root ganglion neurons and dendrites of central neurons. J Biol Chem. 2002; 277:5203–5208. [PubMed: 11739374]

Ettaiche M, Guy N, Hofman P, Lazdunski M, Waldmann R. Acid-sensing ion channel 2 is important for retinal function and protects against light-induced retinal degeneration. J Neurosci. 2004; 24:1005–1012. [PubMed: 14762118]

Feinstein JS, Buzza C, Hurlemann R, Follmer RL, Dahdaleh NS, Coryell WH, Welsh MJ, Tranel D, Wemmie JA. Fear and panic in humans with bilateral amygdala damage. Nat Neurosci. 2013

Gao J, Wu LJ, Xu L, Xu TL. Properties of the proton-evoked currents and their modulation by Ca2+ and Zn2+ in the acutely dissociated hippocampus CA1 neurons. Brain Res. 2004; 1017:197–207. [PubMed: 15261115]

Garcia-Anoveros J, Derfler B, Neville-Golden J, Hyman BT, Corey DP. BNaC1 and BNaC2 constitute a new family of human neuronal sodium channels related to degenerins and epithelial sodium channels. Proc Natl Acad Sci U S A. 1997; 94:1459–1464. [PubMed: 9037075]

Gorman JM, Papp LA, Coplan JD, Martinez JM, Lennon S, Goetz RR, Ross D, Klein DF. Anxiogenic effects of CO2 and hyperventilation in patients with panic disorder. Am J Psychiatry. 1994; 151:547–553. [PubMed: 8147452]

Gregersen N, Dahl HA, Buttenschon HN, Nyegaard M, Hedemand A, Als TD, Wang AG, Joensen S, Woldbye DP, Koefoed P, et al. A genome-wide study of panic disorder suggests the amiloride-sensitive cation channel 1 as a candidate gene. Eur J Hum Genet. 2012; 20:84–90. [PubMed: 21811305]

Grunder S, Chen X. Structure, function, and pharmacology of acid-sensing ion channels (ASICs): focus on ASIC1a. Int J Physiol Pathophysiol Pharmacol. 2010; 2:73–94. [PubMed: 21383888]

Hesselager M, Timmermann DB, Ahring PK. pH Dependency and desensitization kinetics of heterologously expressed combinations of acid-sensing ion channel subunits. J Biol Chem. 2004; 279:11006–11015. [PubMed: 14701823]

Hodges MR, Tattersall GJ, Harris MB, McEvoy SD, Richerson DN, Deneris ES, Johnson RL, Chen ZF, Richerson GB. Defects in breathing and thermoregulation in mice with near-complete absence of central serotonin neurons. J Neurosci. 2008; 28:2495–2505. [PubMed: 18322094]

Holm S. A simple sequentially rejective multiple test procedure. Scandinavian Journal of Statistics. 1979; 6:65–70.

Hruska-Hageman AM, Wemmie JA, Price MP, Welsh MJ. Interaction of the synaptic protein PICK1 (protein interacting with C kinase 1) with the non-voltage gated sodium channels BNC1 (brain Na + channel 1) and ASIC (acid-sensing ion channel). Biochem J. 2002; 361:443–450. [PubMed: 11802773]

Huang C, Hu ZL, Wu WN, Yu DF, Xiong QJ, Song JR, Shu Q, Fu H, Wang F, Chen JG. Existence and distinction of acid-evoked currents in rat astrocytes. Glia. 2010; 58:1415–1424. [PubMed: 20549751]

Hunter AM, Leuchter AF, Power RA, Muthen B, McGrath PJ, Lewis CM, Cook IA, Garriock HA, McGuffin P, Uher R, et al. A genome-wide association study of a sustained pattern of antidepressant response. J Psychiatr Res. 2013; 47:1157–1165. [PubMed: 23726668]

Israely I, Costa RM, Xie CW, Silva AJ, Kosik KS, Liu X. Deletion of the neuron-specific protein delta-catenin leads to severe cognitive and synaptic dysfunction. Curr Biol. 2004; 14:1657–1663. [PubMed: 15380068]

Jasti J, Furukawa H, Gonzales EB, Gouaux E. Structure of acid-sensing ion channel 1 at 1.9 A resolution and low pH. Nature. 2007; 449:316–323. [PubMed: 17882215]

Jiang Q, Li MH, Papasian CJ, Branigan D, Xiong ZG, Wang JQ, Chu XP. Characterization of acid-sensing ion channels in medium spiny neurons of mouse striatum. Neuroscience. 2009; 162:55–66. [PubMed: 19376200]

Johnson PL, Lightman SL, Lowry CA. A functional subset of serotonergic neurons in the rat ventrolateral periaqueductal gray implicated in the inhibition of sympathoexcitation and panic. Ann N Y Acad Sci. 2004; 1018:58–64. [PubMed: 15240352]

Krishtal OA, Osipchuk YV, Shelest TN, Smirnoff SV. Rapid extracellular pH transients related to synaptic transmission in rat hippocampal slices. Brain Res. 1987; 436:352–356. [PubMed: 2829992]

Lavezzi HN, Zahm DS. The mesopontine rostromedial tegmental nucleus: an integrative modulator of the reward system. Basal Ganglia. 2011; 1:191–200. [PubMed: 22163100]

Lecourtier L, Kelly PH. A conductor hidden in the orchestra? Role of the habenular complex in monoamine transmission and cognition. Neurosci Biobehav Rev. 2007; 31:658–672. [PubMed: 17379307]

Lingueglia E, de Weille JR, Bassilana F, Heurteaux C, Sakai H, Waldmann R, Lazdunski M. A modulatory subunit of acid sensing ion channels in brain and dorsal root ganglion cells. J Biol Chem. 1997; 272:29778–29783. [PubMed: 9368048]

Magnotta VA, Heo HY, Dlouhy BJ, Dahdaleh NS, Follmer RL, Thedens DR, Welsh MJ, Wemmie JA. Detecting activity-evoked pH changes in human brain. Proc Natl Acad Sci U S A. 2012; 109:8270–8273. [PubMed: 22566645]

Mazzuca M, Heurteaux C, Alloui A, Diochot S, Baron A, Voilley N, Blondeau N, Escoubas P, Gelot A, Cupo A, et al. A tarantula peptide against pain via ASIC1a channels and opioid mechanisms. Nat Neurosci. 2007; 10:943–945. [PubMed: 17632507]

Mongeluzi DL, Rosellini RA, Ley R, Caldarone BJ, Stock HS. The conditioning of dyspneic suffocation fear. Effects of carbon dioxide concentration on behavioral freezing and analgesia. Behav Modif. 2003; 27:620–636. [PubMed: 14531158]

Page AJ, Brierley SM, Martin CM, Martinez-Salgado C, Wemmie JA, Brennan TJ, Symonds E, Omari T, Lewin GR, Welsh MJ, et al. The ion channel ASIC1 contributes to visceral but not cutaneous mechanoreceptor function. Gastroenterology. 2004; 127:1739–1747. [PubMed: 15578512]

Peng BG, Ahmad S, Chen S, Chen P, Price MP, Lin X. Acid-sensing ion channel 2 contributes a major component to acid-evoked excitatory responses in spiral ganglion neurons and plays a role in noise susceptibility of mice. J Neurosci. 2004; 24:10167–10175. [PubMed: 15537887]

Porsolt RD, Bertin A, Jalfre M. Behavioral despair in mice: a primary screening test for antidepressants. Arch Int Pharmacodyn Ther. 1977; 229:327–336. [PubMed: 596982]

Price MP, Snyder PM, Welsh MJ. Cloning and expression of a novel human brain Na+ channel. J Biol Chem. 1996; 271:7879–7882. [PubMed: 8626462]

R-Core-Team. R: A language and environment for statistical computing. R Foundation for Statistical Computing; Vienna, Austria: 2013. version 2.15.13

Roza C, Puel JL, Kress M, Baron A, Diochot S, Lazdunski M, Waldmann R. Knockout of the ASIC2 channel in mice does not impair cutaneous mechanosensation, visceral mechanonociception and hearing. J Physiol. 2004; 558:659–669. [PubMed: 15169849]

Sewards TV, Sewards MA. The medial pain system: neural representations of the motivational aspect of pain. Brain Res Bull. 2002; 59:163–180. [PubMed: 12431746]

Sherwood TW, Frey EN, Askwith CC. Structure and activity of the acid-sensing ion channels. Am J Physiol Cell Physiol. 2012; 303:C699–C710. [PubMed: 22843794]

Sherwood TW, Lee KG, Gormley MG, Askwith CC. Heteromeric acid-sensing ion channels (ASICs) composed of ASIC2b and ASIC1a display novel channel properties and contribute to acidosis-induced neuronal death. J Neurosci. 2011; 31:9723–9734. [PubMed: 21715637]

Sowers LP, Loo L, Wu Y, Campbell E, Ulrich JD, Wu S, Paemka L, Wassink T, Meyer K, Bing X, et al. Disruption of the non-canonical Wnt gene PRICKLE2 leads to autism-like behaviors with evidence for hippocampal synaptic dysfunction. Mol Psychiatry. 2013

Squassina A, Manchia M, Borg J, Congiu D, Costa M, Georgitsi M, Chillotti C, Ardau R, Mitropoulos K, Severino G, et al. Evidence for association of an ACCN1 gene variant with response to lithium treatment in Sardinian patients with bipolar disorder. Pharmacogenomics. 2011; 12:1559–1569. [PubMed: 21961650]

Stone JL, Merriman B, Cantor RM, Geschwind DH, Nelson SF. High density SNP association study of a major autism linkage region on chromosome 17. Hum Mol Genet. 2007; 16:704–715. [PubMed: 17376794]

Su CY, Menuz K, Carlson JR. Olfactory perception: receptors, cells, and circuits. Cell. 2009; 139:45–59. [PubMed: 19804753]

Takahashi LK, Nakashima BR, Hong H, Watanabe K. The smell of danger: a behavioral and neural analysis of predator odor-induced fear. Neurosci Biobehav Rev. 2005; 29:1157–1167. [PubMed: 16095694]

Veerappa AM, Saldanha M, Padakannaya P, Ramachandra NB. Family-based genome-wide copy number scan identifies five new genes of dyslexia involved in dendritic spinal plasticity. J Hum Genet. 2013

Vralsted VC, Price MP, Du J, Schnizler M, Wunsch AM, Ziemann AE, Welsh MJ, Wemmie JA. Expressing acid-sensing ion channel 3 in the brain alters acid-evoked currents and impairs fear conditioning. Genes Brain Behav. 2011; 10:444–450. [PubMed: 21324060]

Walder RY, Rasmussen LA, Rainier JD, Light AR, Wemmie JA, Sluka KA. ASIC1 and ASIC3 play different roles in the development of Hyperalgesia after inflammatory muscle injury. J Pain. 2010; 11:210–218. [PubMed: 20015700]

Waldmann R, Champigny G, Voilley N, Lauritzen I, Lazdunski M. The mammalian degenerin MDEG, an amiloride-sensitive cation channel activated by mutations causing neurodegeneration in Caenorhabditis elegans. J Biol Chem. 1996; 271:10433–10436. [PubMed: 8631835]

Wemmie JA, Askwith CC, Lamani E, Cassell MD, Freeman JH Jr. Welsh MJ. Acid-sensing ion channel 1 is localized in brain regions with high synaptic density and contributes to fear conditioning. J Neurosci. 2003; 23:5496–5502. [PubMed: 12843249]

Wemmie JA, Chen J, Askwith CC, Hruska-Hageman AM, Price MP, Nolan BC, Yoder PG, Lamani E, Hoshi T, Freeman JH Jr. et al. The acid-activated ion channel ASIC contributes to synaptic plasticity, learning, and memory. Neuron. 2002; 34:463–477. [PubMed: 11988176]

Wemmie JA, Coryell MW, Askwith CC, Lamani E, Leonard AS, Sigmund CD, Welsh MJ. Overexpression of acid-sensing ion channel 1a in transgenic mice increases acquired fear-related behavior. Proc Natl Acad Sci U S A. 2004; 101:3621–3626. [PubMed: 14988500]

Wemmie JA, Price MP, Welsh MJ. Acid-sensing ion channels: advances, questions and therapeutic opportunities. Trends Neurosci. 2006; 29:578–586. [PubMed: 16891000]

Weng JY, Lin YC, Lien CC. Cell type-specific expression of acid-sensing ion channels in hippocampal interneurons. J Neurosci. 2010; 30:6548–6558. [PubMed: 20463218]

Wu LJ, Duan B, Mei YD, Gao J, Chen JG, Zhuo M, Xu L, Wu M, Xu TL. Characterization of acid-sensing ion channels in dorsal horn neurons of rat spinal cord. J Biol Chem. 2004; 279:43716–43724. [PubMed: 15302881]

Xiong ZG, Zhu XM, Chu XP, Minami M, Hey J, Wei WL, MacDonald JF, Wemmie JA, Price MP, Welsh MJ, et al. Neuroprotection in ischemia: blocking calcium-permeable acid-sensing ion channels. Cell. 2004; 118:687–698. [PubMed: 15369669]

Xu TL, Xiong ZG. Dynamic regulation of acid-sensing ion channels by extracellular and intracellular modulators. Curr Med Chem. 2007; 14:1753–1763. [PubMed: 17627513]

Yermolaieva O, Leonard AS, Schnizler MK, Abboud FM, Welsh MJ. Extracellular acidosis increases neuronal cell calcium by activating acid-sensing ion channel 1a. Proc Natl Acad Sci U S A. 2004; 101:6752–6757. [PubMed: 15082829]

Zha XM, Costa V, Harding AM, Reznikov L, Benson CJ, Welsh MJ. ASIC2 subunits target acid-sensing ion channels to the synapse via an association with PSD-95. J Neurosci. 2009; 29:8438–8446. [PubMed: 19571134]

Zha XM, Wemmie JA, Green SH, Welsh MJ. Acid-sensing ion channel 1a is a postsynaptic proton receptor that affects the density of dendritic spines. Proc Natl Acad Sci U S A. 2006; 103:16556–16561. [PubMed: 17060608]

Ziemann AE, Allen JE, Dahdaleh NS, Drebot, Coryell MW, Wunsch AM, Lynch CM, Faraci FM, Howard MA 3rd, Welsh MJ, et al. The amygdala is a chemosensor that detects carbon dioxide and acidosis to elicit fear behavior. Cell. 2009; 139:1012–1021. [PubMed: 19945383]

Zou DJ, Chesler A, Firestein S. How the olfactory bulb got its glomeruli: a just so story? Nat Rev Neurosci. 2009; 10:611–618. [PubMed: 19584894]

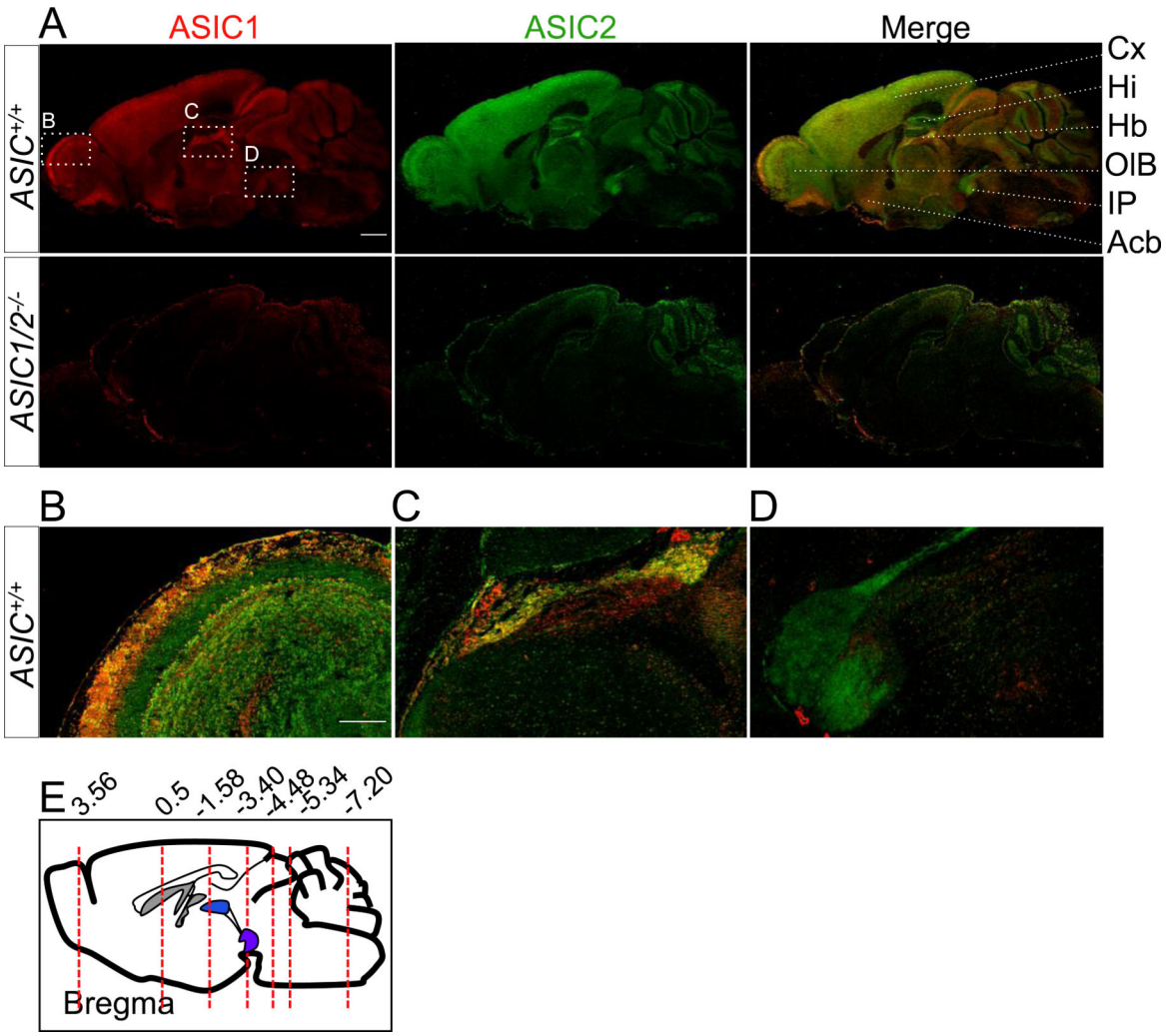

Figure 1. Co-immunolocalization of ASIC1 and ASIC2 in mouse brain

A. Co-immunostaining of ASIC1 (red) and ASIC2 (green) in para-sagittal sections of mouse brain from *ASIC*$^{+/+}$ and *ASIC1/2*$^{-/-}$ mice. Scale bar represents 1 mm. Enlarged images of the olfactory bulb (**B**), habenula (**C**), and interpeduncular nucleus (**D**). Scale bar represents 250 μm. **E**. Coronal sections were cut at various bregma (red dotted lines) for further staining. Acb, accumbens nucleus. Cx, cortex; Hb, habenula; Hi, hippocampus; IP, interpeduncular nucleus; OlB, olfactory bulb.

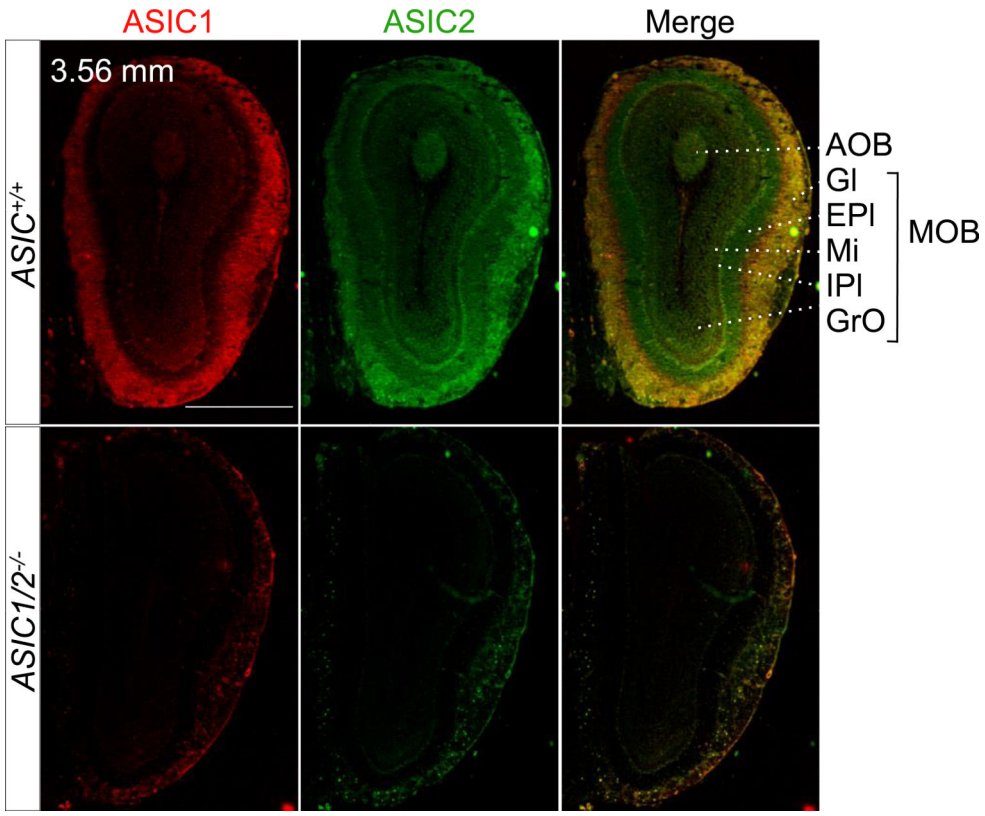

Figure 2. Co-immunolocalization of ASIC1 and ASIC2 in the olfactory bulb

Co-immunostaining of ASIC1 (red) and ASIC2 (green) in coronal sections of the main and accessory olfactory bulbs from *ASIC1*$^{+/+}$ and *ASIC1/2*$^{-/-}$ mice. Sections were cut at bregma 3.56 mm of *ASIC*$^{+/+}$ and *ASIC1/2*$^{-/-}$ mouse brains as indicated. Scale bar represents 1 mm. AOB, accessory olfactory bulb; EPl, external plexiform layer; Gl, glomerular layer; GrO, granule layer; IPl, internal plexiform layer; MOB, main olfactory bulb; Mi, mitral layer.

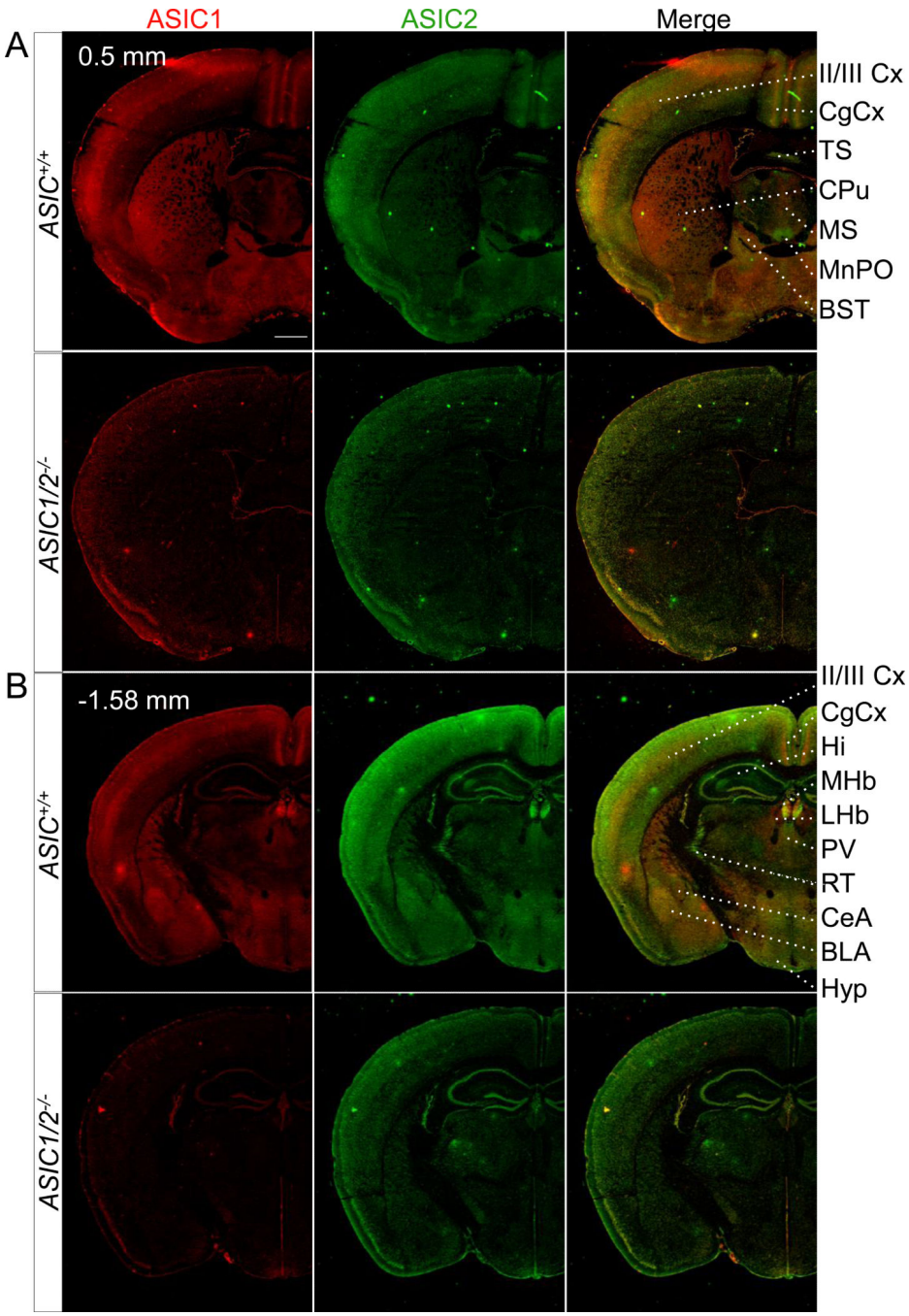

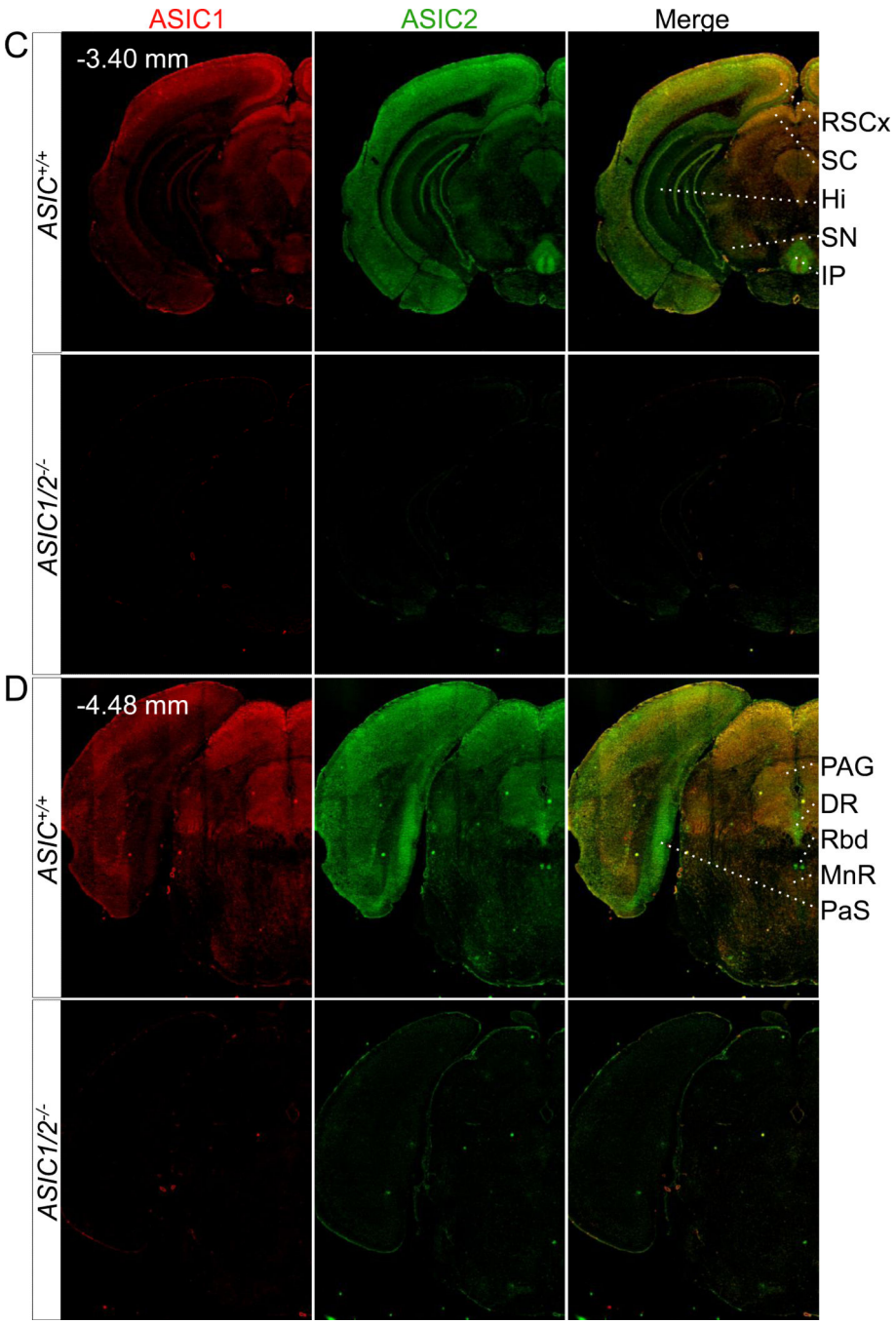

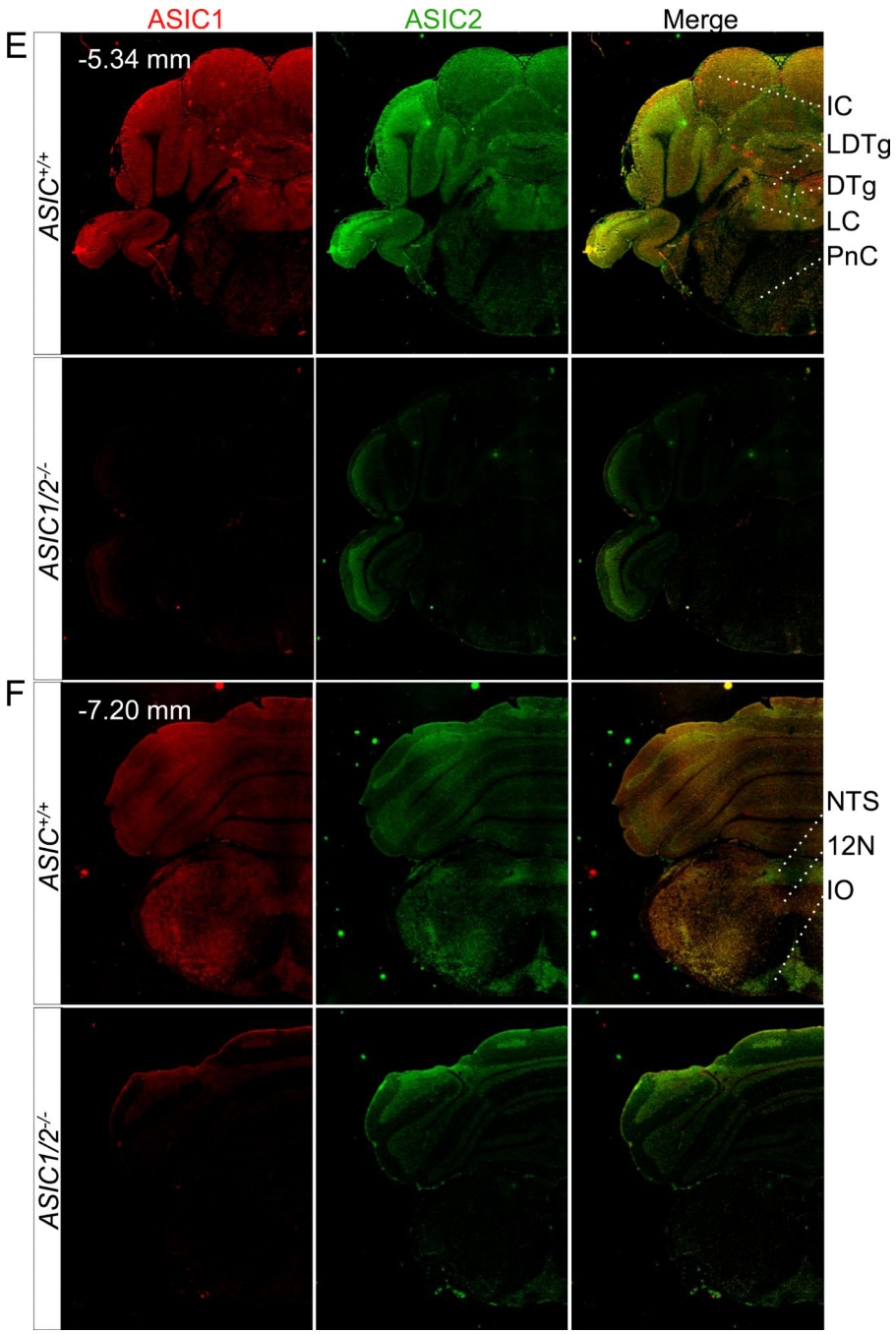

Figure 3. Co-immunolocalization of ASIC1 and ASIC2 in specific coronal sections throughout the brain

Co-immunostaining of ASIC1 (red) and ASIC2 (green) in coronal sections of *ASIC*$^{+/+}$ and *ASIC1/2*$^{-/-}$ mouse brains, cut at bregma indicated in A, B, C, D, E, and F. Scale bar represents 800 μm. BLA, basolateral amygdala; BST, bed nucleus of the stria terminalis; CPu, caudate-putamen; CeA, central amygdala; CgCx, cingulate cortex; DR, dorsal raphe; DTg, dorsal temental nucleus, pericentral part; Hi, hippocampus; 12N, hypoglossal nucleus; Hyp, hypothalamus; IC, inferior colliculus; IO, inferior olive. IP, interpeduncular nucleus; LDTg, lateral dorsal tegmental nucleus; LHb, lateral habenula; II/III Cx, layer II/III in cortex; LC, locus cerulius; MHb, medial habenula; ; MS, medial septal nucleus; MnPO, median preoptic nucleus; MnR, median raphe; NTS, nucleus of the solitary tract; PaS, parasubiculum; PV, paraventricular thalamic nucleus; PAG, periaqueductal gray; PnC,

pontine reticular nucleus; RT, reticular thalamic nucleus; RSCx, retrosplenial cortex; Rbd, rhabdoid nucleus; SN, substantia nigra; SC, superior colliculus; TS, triangular segment.

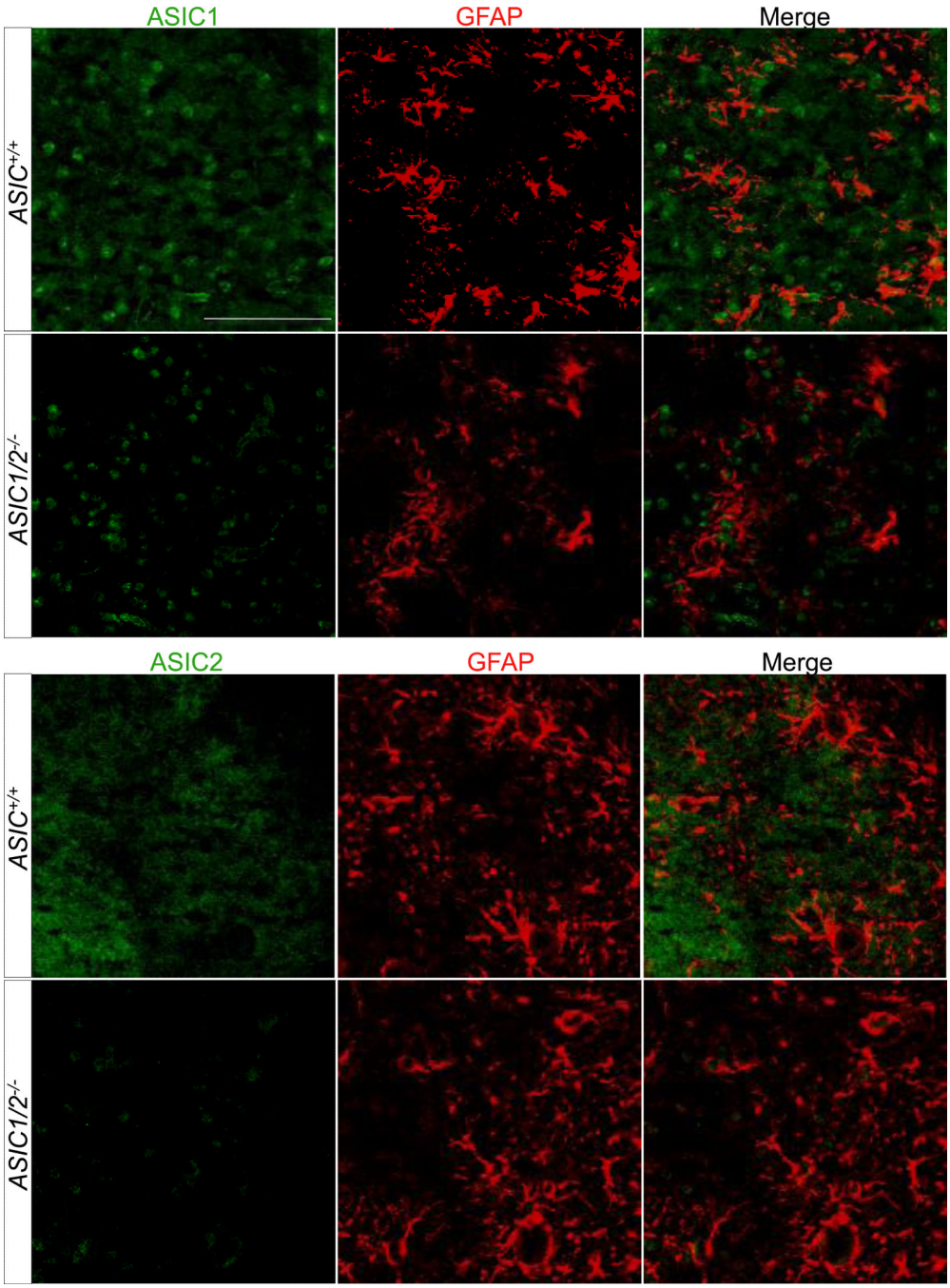

Figure 4. Co-immunolocalization of ASIC1 and ASIC2 with glial fibrillary acidic protein (GFAP)

Co-immunostaining of ASIC1 and ASIC2 (both in green) with glial fibrillary acidic protein (GFAP) (red) in regions of mouse brain where ASIC1 and ASIC2 are highly expressed (ASIC1 in the PAG and ASIC2 in the IPN). Scale bar represents 100 μm.

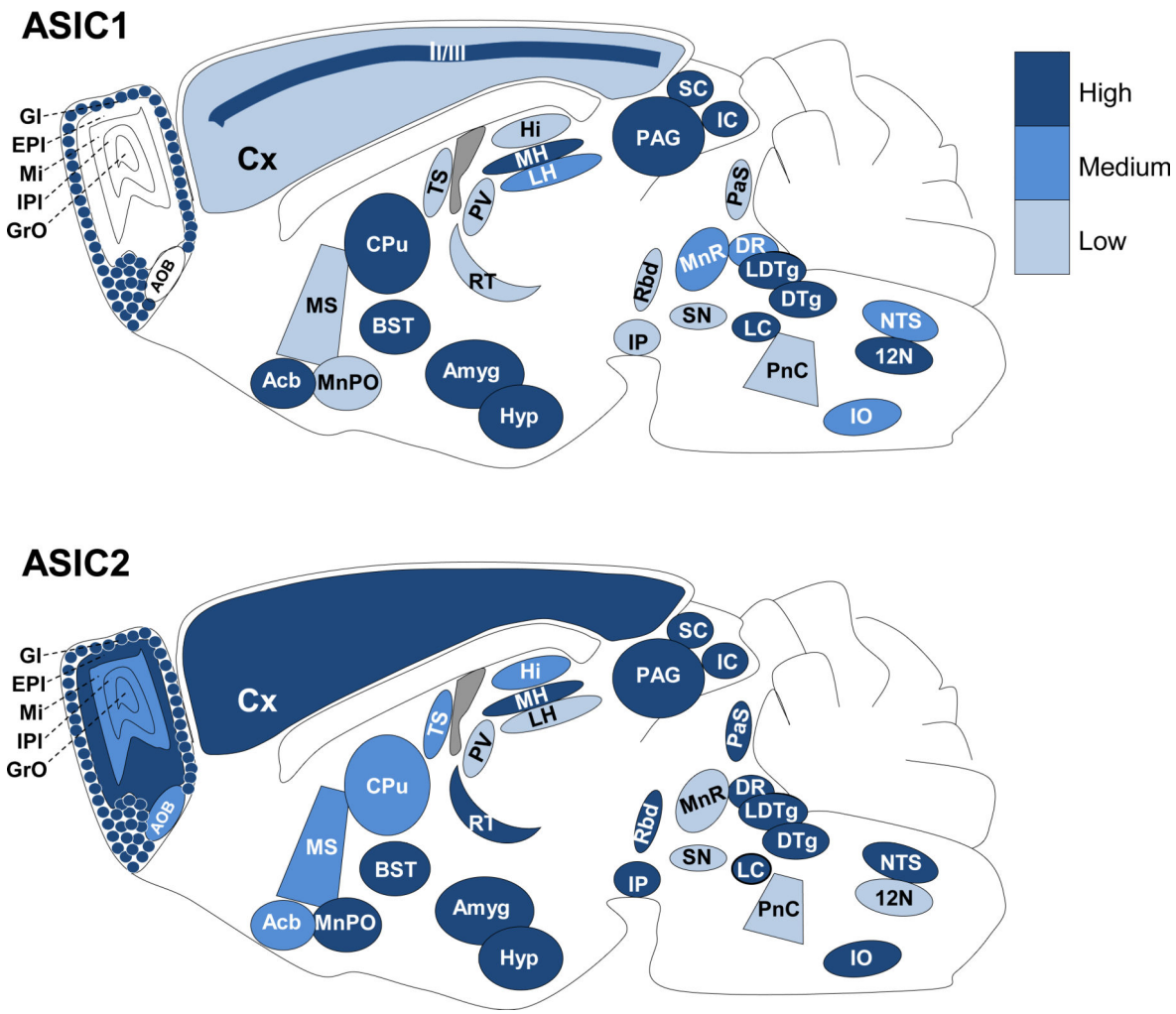

Figure 5. Depiction of ASIC1 and ASIC2 localization throughout the brain

Brain schematic depicting relative levels of immunostaining of ASIC1 (top) and ASIC2 (bottom) in the indicated structures in mouse brain.

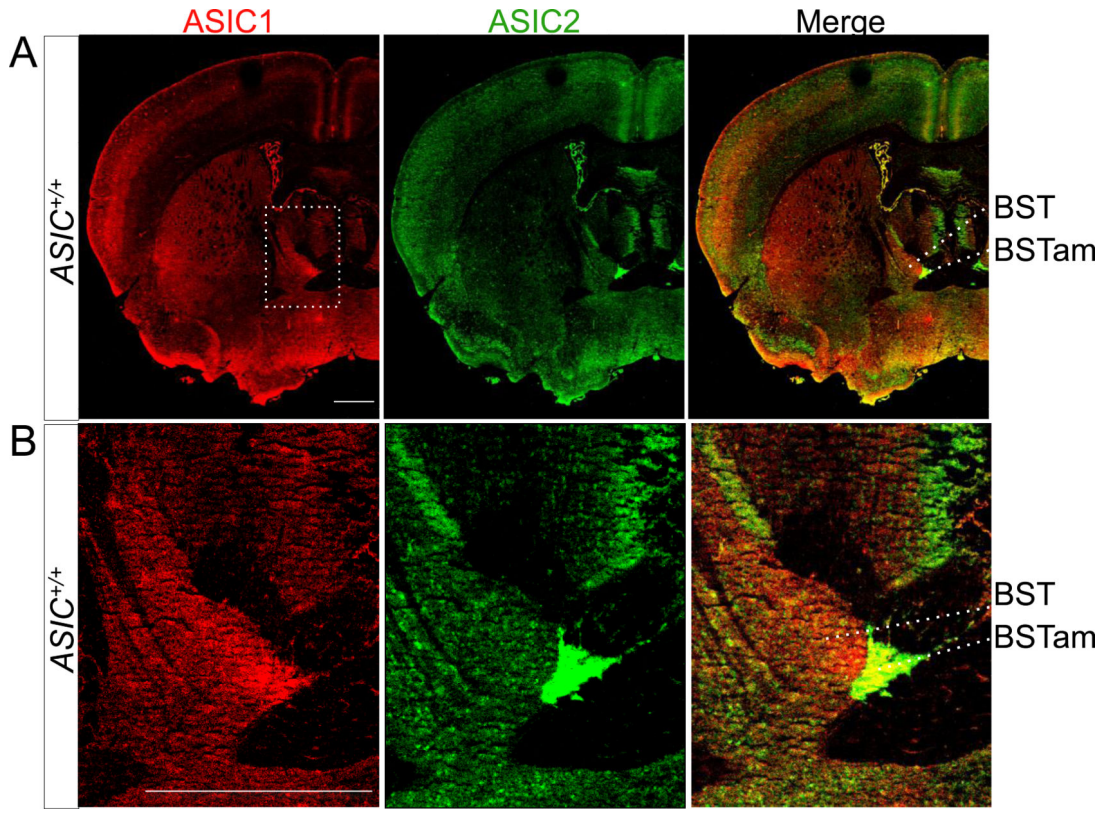

Figure 6. Co-immunolocalization of ASIC1 and ASIC2 in the BST

A. Co-immunostaining of ASIC1 (red) and ASIC2 (green) in coronal section of mouse forebrain. **B.** Enlarged image of the anterior medial area of the BST. Scale bar in (**A**) and (**B**) represents 800 μm.

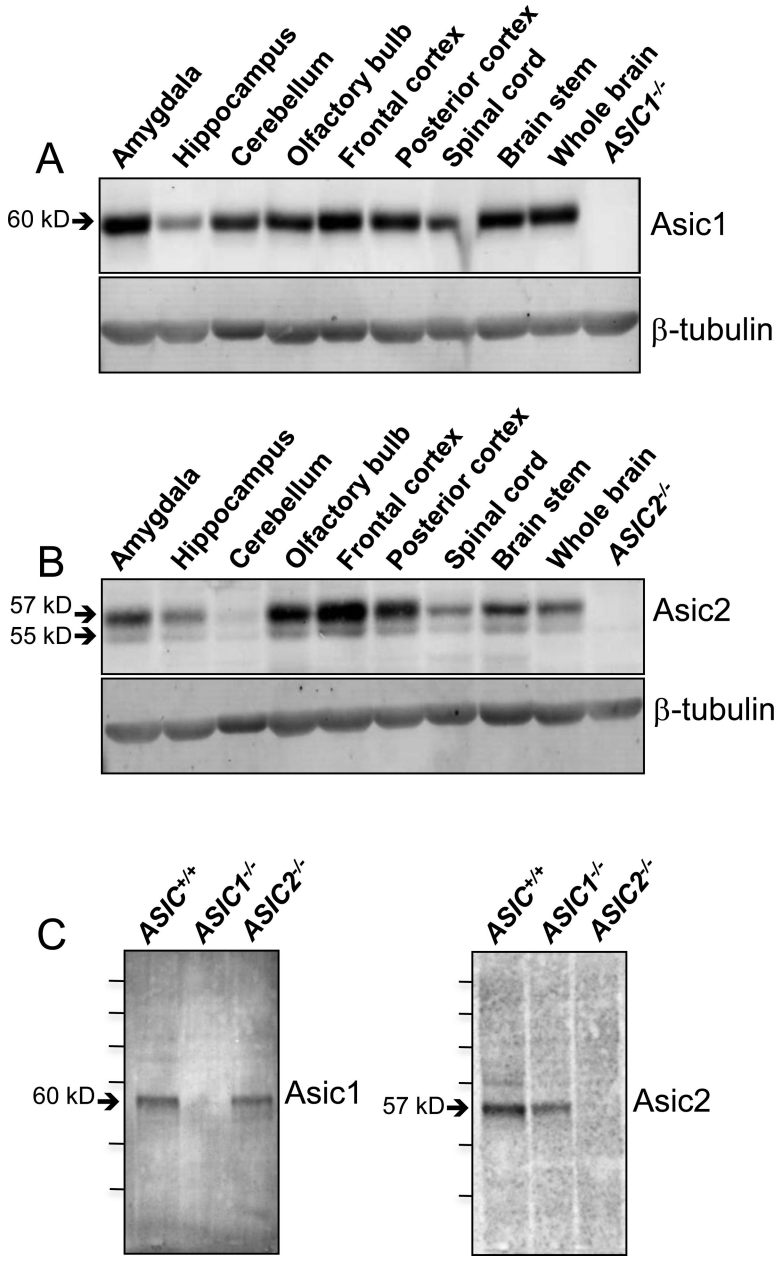

Figure 7. Western blot analysis of ASIC1 and ASIC2 in protein extracts of dissected regions of mouse brain

A. Western blotting with anti-ASIC1 antibody; right lane contained whole brain lysate from an *ASIC1*$^{-/-}$ brain. **B.** Western blotting with anti-ASIC2 antibody; right lane contained whole brain lysate from an *ASIC2*$^{-/-}$ brain. Blotting for ß-tubulin served as a control for the amount of protein loaded in each lane. **C.** Western blotting of whole brain lysate from *ASIC*$^{+/+}$, *ASIC1*$^{-/-}$, and *ASIC2*$^{-/-}$ mice with anti-ASIC1 or anti-ASIC2 antibody as indicated. Protein MW markers, from top to bottom are as follows in kD: 250, 150, 100, 75, 50, 37.

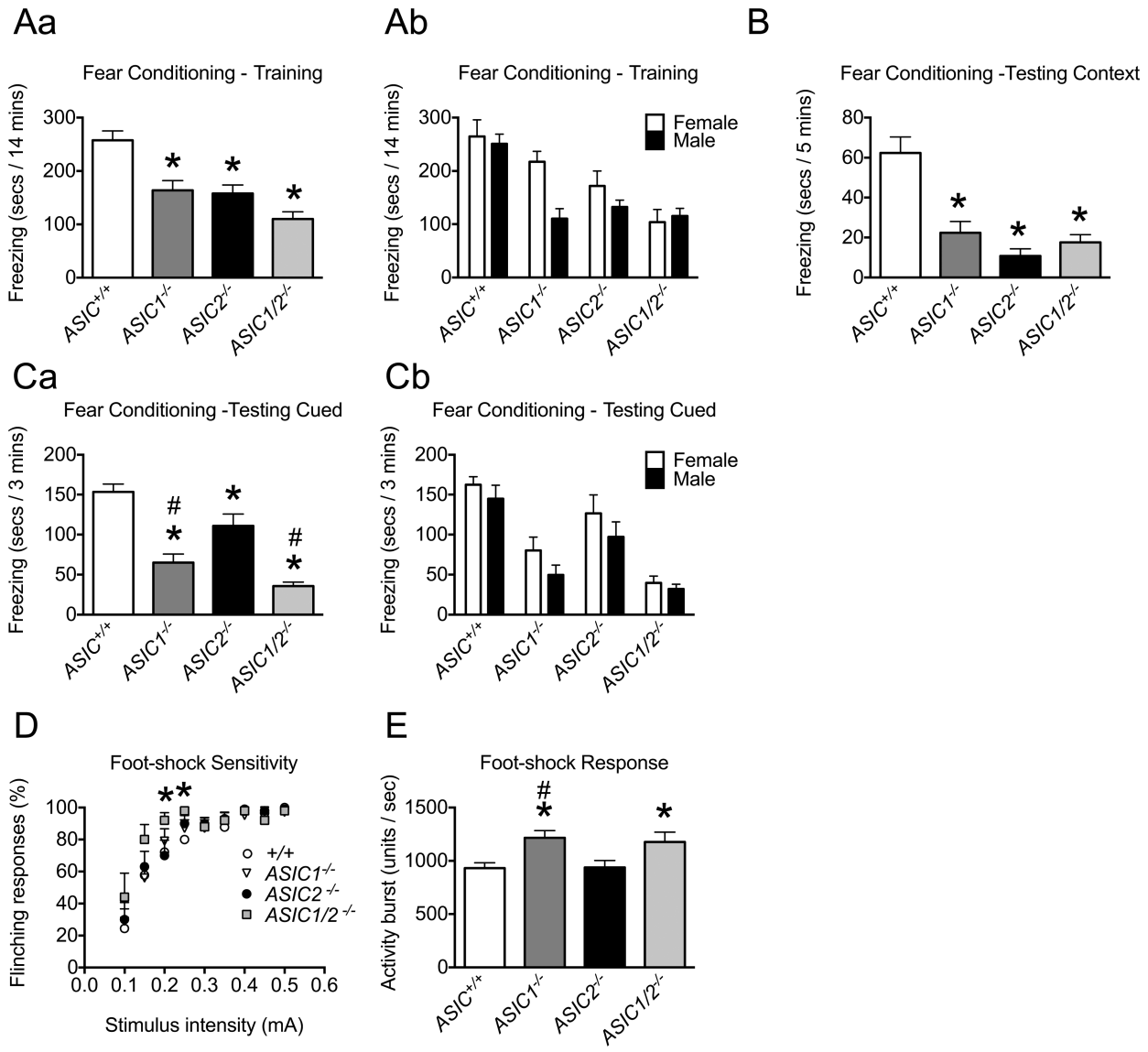

Figure 8. Behavioral analyses of *ASIC*$^{+/+}$ and *ASIC*$^{-/-}$ mice in conditioned fear assays

A. Context and cue fear training. *ASIC1*$^{-/-}$, *ASIC2*$^{-/-}$, and *ASIC1/2*$^{-/-}$ mice froze significantly less than *ASIC*$^{+/+}$ mice during the 14 min training period (* difference compared with *ASIC*$^{+/+}$ ($P < 0.05$), post-hoc Holm's correction; *ASIC*$^{+/+}$, $n = 31$, 16 male, 15 female; *ASIC1*$^{-/-}$, $n = 20$, 10 male, 10 female; *ASIC2*$^{-/-}$, $n = 17$, 9 male, 8 female; *ASIC1/2*$^{-/-}$, $n = 21$, 11 male, 10 female). Male and female data are reported together in **Aa** and separately in **Ab**. **B.** Context fear testing. *ASIC1*$^{-/-}$, *ASIC2*$^{-/-}$, and *ASIC1/2*$^{-/-}$ mice froze significantly less than *ASIC*$^{+/+}$ mice during 5 min testing to context (* difference compared with *ASIC*$^{+/+}$ ($P < 0.05$), post-hoc Holm's correction; *ASIC*$^{+/+}$, $n = 26$, 14 male, 12 female; *ASIC1*$^{-/-}$, $n = 20$, 10 male, 10 female; *ASIC2*$^{-/-}$, $n = 17$, 9 male, 8 female; *ASIC1/2*$^{-/-}$, $n = 12$, 6 male, 6 female). **C**. Auditory cue fear testing. *ASIC1*$^{-/-}$, *ASIC2*$^{-/-}$, and *ASIC1/2*$^{-/-}$ mice froze significantly less than *ASIC*$^{+/+}$ mice, and *ASIC1*$^{-/-}$ and *ASIC1/2*$^{-/-}$ froze significantly less than *ASIC2*$^{-/-}$ mice during the 3 min tone-on period of the 10 min session; freezing during the tone-off period of the session was negligible (* difference compared with *ASIC*$^{+/+}$ ($P < 0.05$), # difference compared with *ASIC2*$^{-/-}$ ($P < 0.05$), post-hoc Holm's correction; *ASIC*$^{+/+}$, $n = 31$, 16 male, 15 female; *ASIC1*$^{-/-}$, $n = 20$, 10 male, 10 female; *ASIC2*$^{-/-}$, $n = 17$, 9 male, 8 female; *ASIC1/2*$^{-/-}$, $n = 21$, 11 male, 10 female). Male and female data are reported together in **Ca** and separately in **Cb**. **D.** Foot-shock sensitivity. Percentage of foot-shock stimuli that elicited a flinching response. Foot-shocks were delivered at increasing levels of

intensity; there were 10 presentations at each intensity. There were significant differences in foot-shock sensitivity between *ASIC*$^{+/+}$ and *ASIC1/2*$^{-/-}$ at intensities of 0.20 mA and 0.25 mA (* difference compared with *ASIC*$^{+/+}$ ($P < 0.05$), post-hoc Bonferroni correction; *ASIC*$^{+/+}$, $n = 9$, 9 male; *ASIC1*$^{-/-}$, $n = 10$, 10 male; *ASIC2*$^{-/-}$, $n = 10$, 10 male; *ASIC1/2*$^{-/-}$, $n = 5$, 5 male). **E.** Foot-shock response. The unconditioned activity burst during the first second following the initial foot-shock (measured using the motion index function of the Video Freeze software) was used to quantify the response to foot-shock. *ASIC1*$^{-/-}$ and *ASIC1/2*$^{-/-}$ mice had a significantly greater activity burst than *ASIC*$^{+/+}$ mice and *ASIC1*$^{-/-}$ mice had a significantly greater activity burst than *ASIC2*$^{-/-}$ mice (* difference compared with *ASIC*$^{+/+}$ ($P < 0.05$), # difference compared with *ASIC2*$^{-/-}$ ($P < 0.05$), post-hoc Holm's correction; *ASIC*$^{+/+}$, $n = 31$, 16 male, 15 female; *ASIC1*$^{-/-}$, $n = 20$, 10 male, 10 female; *ASIC2*$^{-/-}$, $n = 17$, 9 male, 8 female; *ASIC1/2*$^{-/-}$, $n = 21$, 11 male, 10 female). Values are expressed as mean + SEM. A detailed statistical analysis for all parameters is provided in Table S1.

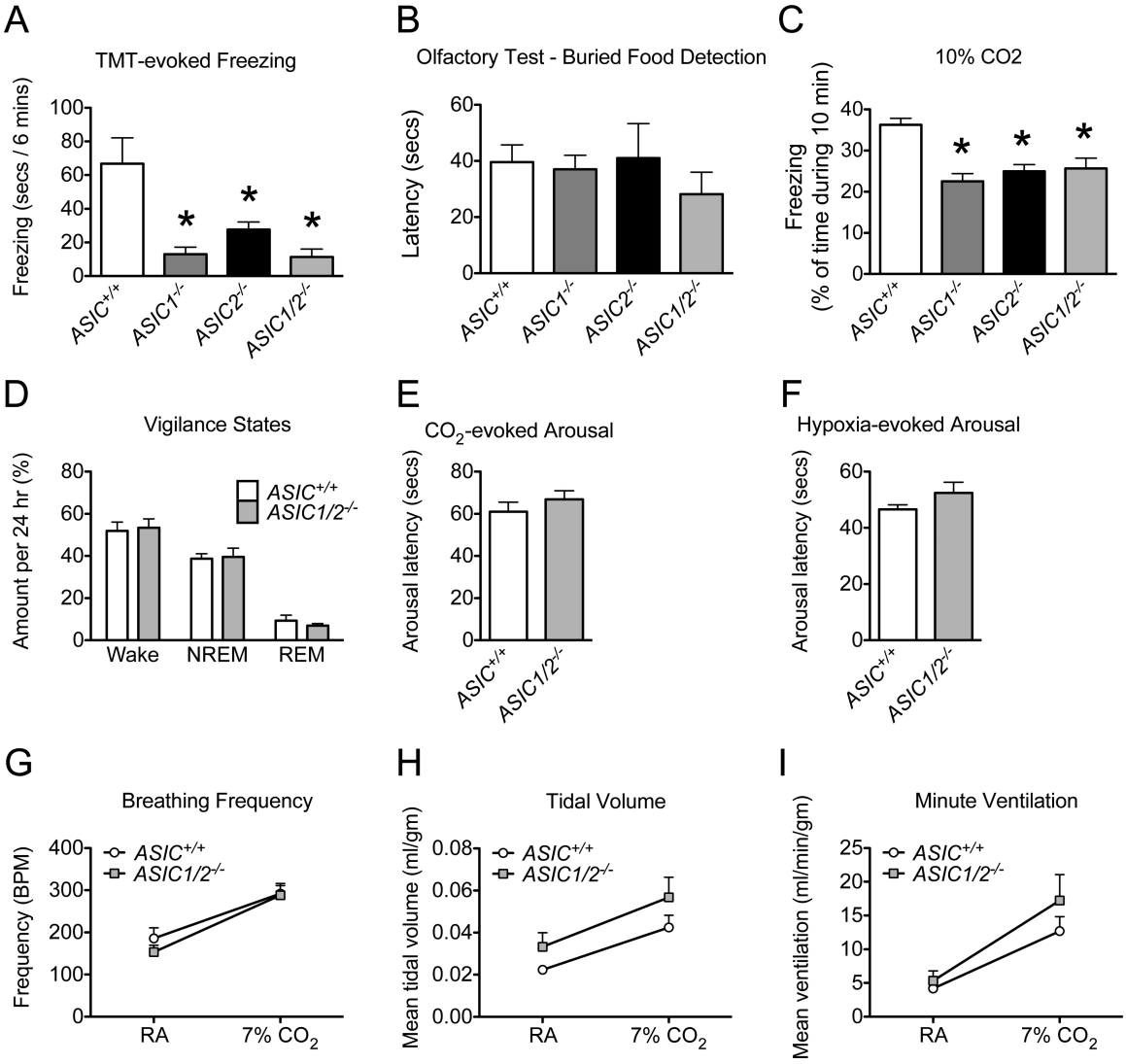

Figure 9. Behavioral analyses of *ASIC*$^{+/+}$ and *ASIC*$^{-/-}$ mice in assays of innate fear and CO_2-evoked responses

A. Unconditioned fear. *ASIC1*$^{-/-}$, *ASIC2*$^{-/-}$, and *ASIC1/2*$^{-/-}$ mice froze significantly less than *ASIC*$^{+/+}$ mice in response to TMT during the 6 min trial period (* difference compared with *ASIC*$^{+/+}$ ($P < 0.05$), post-hoc Holm's correction; *ASIC*$^{+/+}$, $n = 9$, 5 male, 4 female; *ASIC1*$^{-/-}$, $n = 9$, 4 male, 5 female; *ASIC2*$^{-/-}$, $n = 8$, 4 male, 4 female; *ASIC1/2*$^{-/-}$, $n = 5$, 2 male, 3 female). **B.** Olfaction. There were no statistical differences in the latency to find a buried food pellet between genotypes or sex (*ASIC*$^{+/+}$, $n = 7$, 3 male, 4 female; *ASIC1*$^{-/-}$, $n = 7$, 3 male, 4 female; *ASIC2*$^{-/-}$, $n = 11$, 6 male, 5 female; *ASIC1/2*$^{-/-}$, $n = 11$, 6 male, 5 female). **C.** CO_2-evoked freezing. *ASIC1*$^{-/-}$, *ASIC2*$^{-/-}$, and *ASIC1/2*$^{-/-}$ mice spent a significantly smaller percentage of time freezing than *ASIC*$^{+/+}$ mice during the 10 min trial period when exposed to 10% CO_2 (* difference compared with *ASIC*$^{+/+}$ ($P < 0.05$), post-hoc Holm's correction; *ASIC*$^{+/+}$, $n = 18$, 18 male; *ASIC1*$^{-/-}$, $n = 14$, 14 male; *ASIC2*$^{-/-}$, $n = 16$, 16 male; *ASIC1/2*$^{-/-}$, $n = 12$, 12 male). **D.** Sleep/wake patterns. % of time spent in each vigilance state - awake (wake), non-rapid eye movement sleep (NREM), and rapid eye movement sleep (REM) - during the 24 h trial period. There was no statistical evidence of differences between genoytpes in % of time spent in NREM vs. wake states. We only considered NREM and wake states in the analysis of vigilance states since the total of REM, NREM, and wake times were constrained to 24 h. (*ASIC*$^{+/+}$, $n = 8$, 8 male; *ASIC1/2*$^{-/-}$, $n = 8$, 8 male.) **E.** CO_2-evoked arousal. There was no statistical evidence of differences between genotypes in latency to arousal when placed in 7% CO_2. (*ASIC*$^{+/+}$, $n = 8$, 8 male; *ASIC1/2*$^{-/-}$, $n = 8$, 8 male). **F.** O_2-evoked arousal. There

was no statistical evidence of differences between genotypes in latency to arousal when placed in 5% O_2. (*ASIC*$^{+/+}$, *n* = 8, 8 male; *ASIC1/2*$^{-/-}$, *n* = 8, 8 male.) **G, H, and I.** There was no statistical evidence of differences between genotypes in breathing frequency (breaths/min) (**G**), tidal volume (normalized to weight) (**H**), or ventilation (normalized to weight) (**I**) while breathing room air (RA) and 7%CO_2. (*ASIC*$^{+/+}$, *n* = 8, 8 male; *ASIC1/2*$^{-/-}$, *n* = 8, 8 male.**)** Values are expressed as mean + SEM. A detailed statistical analysis for all parameters is provided in Table S1.

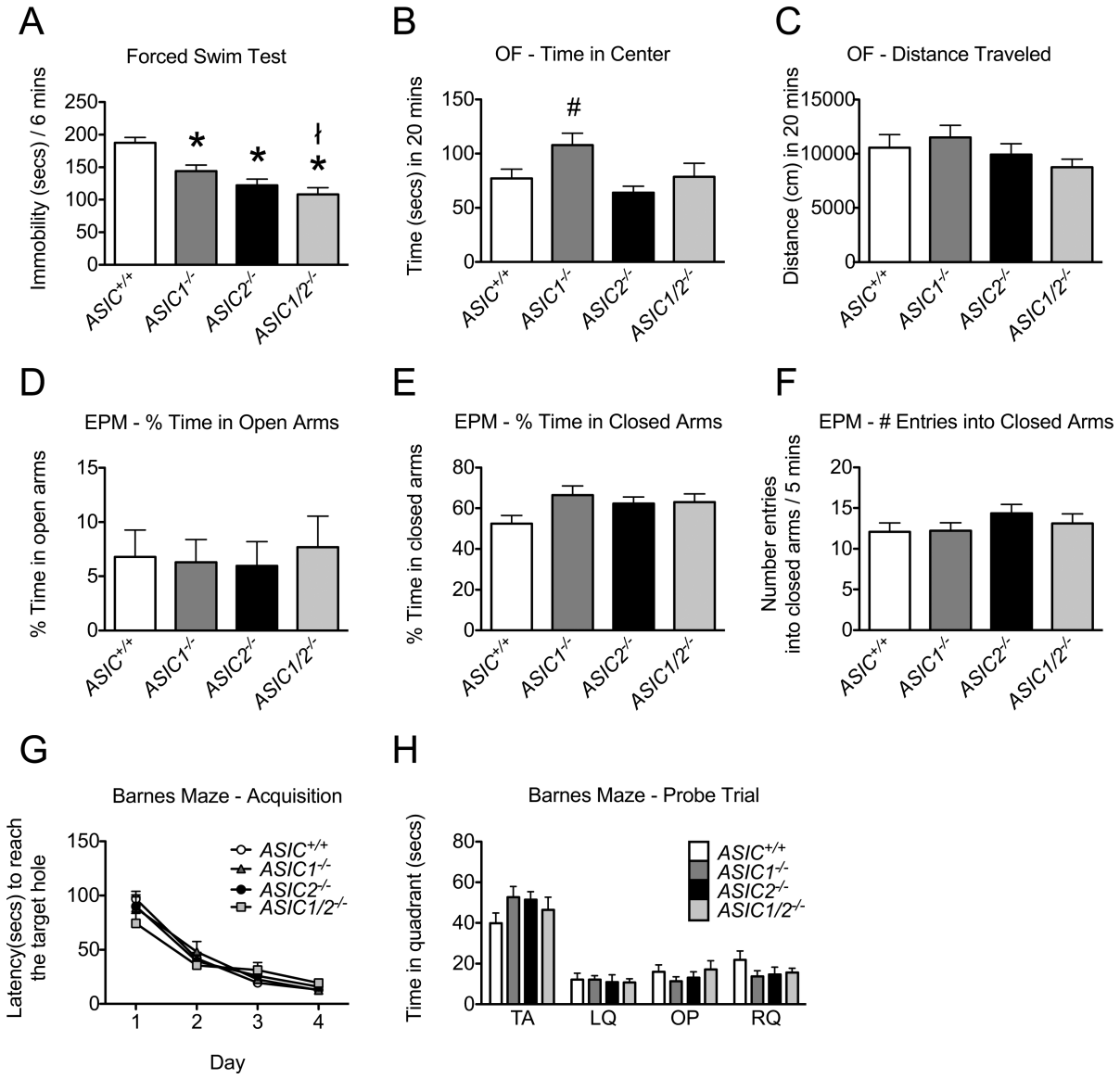

Figure 10. Behavioral analyses of *ASIC*$^{+/+}$ and *ASIC*$^{-/-}$ mice in forced swim, open field, elevated plus maze, and Barnes maze assays

A. Depression-related behavior. *ASIC1*$^{-/-}$, *ASIC2*$^{-/-}$, and *ASIC1/2*$^{-/-}$ mice spent less time immobile than *ASIC*$^{+/+}$ mice, and *ASIC1*$^{-/-}$ mice spent less time immobile than *ASIC1/2*$^{-/-}$ mice during the 6 min trial period of the Porsolt forced swim test (* difference compared with *ASIC*$^{+/+}$ ($P < 0.05$), ł difference compared with *ASIC1*$^{-/-}$($P < 0.05$), post-hoc Holm's correction; *ASIC*$^{+/+}$, *n* = 28, 14 male, 14 female; *ASIC1*$^{-/-}$, *n* = 27, 16 male, 11F; *ASIC2*$^{-/-}$, *n* = 25, 12 male, 13 female; *ASIC1/2*$^{-/-}$, *n* = 23, 12 male, 11 female). Average weights of different groups: *ASIC*$^{+/+}$, 21.5 g; *ASIC1*$^{-/-}$, 23.3 g; *ASIC2*$^{-/-}$, 22.8 g; *ASIC1/2*$^{-/-}$, 20.7g. **B, C.** Open field test. *ASIC1*$^{-/-}$ mice spent more time than *ASIC2*$^{-/-}$ mice in the central zone of an open field area during a 20 min trial period (# difference compared with *ASIC2*$^{-/-}$ ($P < 0.05$), post-hoc Holm's correction) (**B**). There was no statistical evidence of differences in the distance travelled in an open field between genotypes or sex during this trial period (**C**). (*ASIC*$^{+/+}$, *n* = 21, 7 male, 14 female; *ASIC1*$^{-/-}$, *n* = 26, 14 male, 12 female; *ASIC2*$^{-/-}$, *n* = 28, 14 male, 14 female; *ASIC1/2*$^{-/-}$, *n* = 19, 9 male, 10 female.) **D, E,** and **F.** Elevated plus maze. There was no statistical evidence of differences between genotypes or sex in % time animals spent in open (**D**) or closed (**E**) arms of the elevated plus maze or the number of entries into the closed arms (**F**) during a 5 min trial period. (*ASIC*$^{+/+}$, *n* = 11, 5 male, 6 female; *ASIC1*$^{-/-}$, *n* = 9, 5 male, 4

female; *ASIC2*$^{-/-}$, *n* = 11, 6 male, 5 female; *ASIC1/2*$^{-/-}$, *n* = 8, 3 male, 5 female.) **G, H.** Barnes Maze. There was no statistical evidence of differences between genotypes or sex in latency to reach the target hole during the training days (**G**). (*ASIC*$^{+/+}$, *n* = 12, 6 male, 6 female; *ASIC1*$^{-/-}$, *n* = 12, 6 male, 6 female ; *ASIC2*$^{-/-}$, *n* = 12, 6 male, 6 female; *ASIC1/2*$^{-/-}$, *n* = 11, 5 male, 6 female.) There was no statistical evidence of differences between genotypes in time spent in specific quadrants during the probe test following the training days (**H**). TA indicates target quadrant; LQ indicates adjacent left quadrant; OP indicates opposite quadrant; RQ indicates adjacent right quadrant. (*ASIC*$^{+/+}$, *n* = 10, 4 male, 6 female; *ASIC1*$^{-/-}$, *n* = 10, 4 male, 6 female; *ASIC2*$^{-/-}$, *n* = 10, 5 male, 5 female; *ASIC1/2*$^{-/-}$, *n* = 11, 5 male, 6 female.) Values are expressed as mean + SEM. A detailed statistical analysis for all parameters is provided in Table S1.